NTNU
Norwegian University of
Science and Technology

Sliding Mode Control of an Electro-Pneumatic Clutch Actuator

Erlend Helgeland

Master of Science in Engineering Cybernetics
Submission date: May 2008
Supervisor: Tor Arne Johansen, ITK
Co-supervisor: Christian Bratli, Kongsberg Automotive
Hege Langjord, ITK

Norwegian University of Science and Technology
Department of Engineering Cybernetics

Problem Description

Robustness is very important in safety critical automotive applications, such as clutch actuation. We must thus choose the control strategy giving the best tradeoffs between accuracy and robustness. In this project, the student is invited to design and test a sliding mode controller and compare its performance to that of a PD controller. Sliding mode control is interesting because of its robustness when faced with bounded modeling errors. Sliding mode control is also likely to be well suited for the on/off type of control we see when using on/off pneumatic valves to control the actuator.

The master thesis will contain:

Design of a sliding mode controller based on Arie Levant's work and the observer Erlend Helgeland created during his project work 2007.

Simulation study of sliding mode controller and PD controller.

Test of both sliding mode controller and PD controller in a real truck at Kongsberg Automotive.

Comparison of PD controller vs. sliding mode controller.

Robustness discussion. PD vs. sliding mode

Assignment given: 07. January 2008
Supervisor: Tor Arne Johansen, ITK

Abstract

This report investigates proportional-derivative (PD) controller and different versions of sliding mode controllers, including a 2-sliding mode controller invented by Arie Levant, applied to a pneumatic actuator on a truck clutch,

The purpose of the clutch system is to develop a transmission system consisting of a normal clutch and transmission controlled automatically as an automatic gearbox, called automated manual transmission. The goal is to increase driver comfort and performance, as well as reduce fuel consumption.

It is put an effort in implementing an accurate simulation model of the clutch system in Matlab Simulink. The model output includes clutch position, velocity and acceleration, actuator chamber pressure and temperature. The accuracy of the model developed is assumed to be accurate enough for control design.

The only measurement available is position measurement, because more sensors increase cost. The measurement noise is low, which enables direct use of the position measurement for control. For the controllers and other parts of the control system that is dependent on velocity, acceleration or pressure estimates, the measurement has to be differentiated. Differentiation of noisy signals is problematic, therefore filters have to be used. In this report a first order low pass filter differentiator is compared to a robust differentiator, which is inspired by higher order sliding modes and developed by Arie Levant. The reason for comparing it with a very simple filter is the simplicity of the first order filter. It is easy to understand and tune. The performance of the robust differentiator is in this application not better than the first order filter. Therefore the first order filter is used in the tests.

A simplified version of the simulation model is used in the design of the controllers. A PD controller with limited derivative action is tuned on the basis of a linearized version of the control model. PD controllers have turned out to perform well and is suitable for comparison, because they are independent of measurement filters, well known and have well established design methods. The PD controller is compared to different sliding mode controllers. The most promising sliding mode controller, which is a boundary layer controller with variable boundary layer width, is tested thoroughly on the simulation model. Different tests where the simulation model parameters are altered, are performed to investigate the robustness and performance properties of the controllers.

The most promising sliding mode controller were supposed to be tested against the PD controller on a test truck at Kongsberg Automotive. New and faster valves were supposed to be tested in the truck. Unfortunately they did not arrived in time for the test and in addition,

the driver circuit of the older and slower valves broke down under the test startup. Therefore the real tests could not be accomplished. A brief overview of the planned field tests is given.

The PD controller and sliding mode controller are compared in a view focusing on robustness. It is found that the ideal sliding mode controller is highly robust, but not usable in practise for this application.

The developed variable boundary layer sliding mode controller performs better than the PD controller on the simulation model. The reason may be that it is tailored to the reference trajectory used, as opposed to the PD controller which is tuned using Bode diagrams, gain and phase margins. Both controllers possess approximately the same robustness properties.

Preface

This master thesis contains the work and results of the 10th semester of the master's degree of Engineering Cybernetics at the Norwegian University of Science and Technology (NTNU). The project assignment is given by Kongsberg Automotive ASA and is based on the doctoral thesis of Glenn-Ole Kaasa [6].

Thanks to the advisors Tor Arne Johansen, NTNU, and Christian Bratli, Kongsberg Automotive. Co-advisor was Hege Langjord, NTNU, who gave answers to both simple and intricate questions. They have all contributed to a better understanding of the problem.

The author would like to thank his fellow students Jan-Egil Wagnild, Gjermund Tomasgård, Martin Kivle and Kjetil Hodne for great help and good answers to all sorts of questions. Especially thanks to Thomas Rognmo and Henrik Helgesen for their help regarding linear control and Matlab implementation.

Erlend Helgeland
Trondheim May 29, 2008

Contents

Chapter 1

Introduction

1.1 Background

Large amounts of goods are transported by trucks in the contemporary society. If it is possible to save a smaller amount of fuel per truck, it would be beneficial for both the owner and the community. In these days of increased focus on emissions and climate, it is important to have a green profile towards customers.

One way of reducing fuel consumption is to develop more efficient truck transmission systems. It is advantageous to use automatic transmission for the heavy-duty truck industry for this purpose, and it will increase driver comfort, especially during city driving, as well. A trend in the truck industry is to develop automatic or semi-automatic transmissions.

Normal automatic transmissions, similar to those used in private cars, are undesirable due to efficiency. It is therefore preferable to use automated manual transmission, i.e. a normal manual transmission operated by a computer, but other variants have also been attempted. One of the key components in automated transmission is the clutch actuator and its control system. Clutch control will be the subject of this report.

Trucks are usually equipped with a pneumatic system. Therefore it is advantageous with respect to cost to use a pneumatic actuator to control the clutch position. An alternative is to use a hydraulic actuator. Hydraulic actuators are simpler to model and control, but more expensive.

1.2 System description

The control problem consists of making the distance between the clutch friction plates track a time varying reference, by controlling the pressure inside a pneumatic actuator with two valves. The clutch plate mounted on the flywheel of the motor is fixed. Therefore the distance between the two plates is given by the position of the plate mounted on the drive shaft of the truck.

The two friction plates that are pushed together by a nonlinear spring. The spring force constitutes the main nonlinearity in the system.

The clutch actuator consist of a piston which separates a cylinder into two chambers. The piston is connected to the clutch by a lever arm. Figure 1.1 shows the actuator and clutch system. Figure 2.1 shows a schematic drawing it.

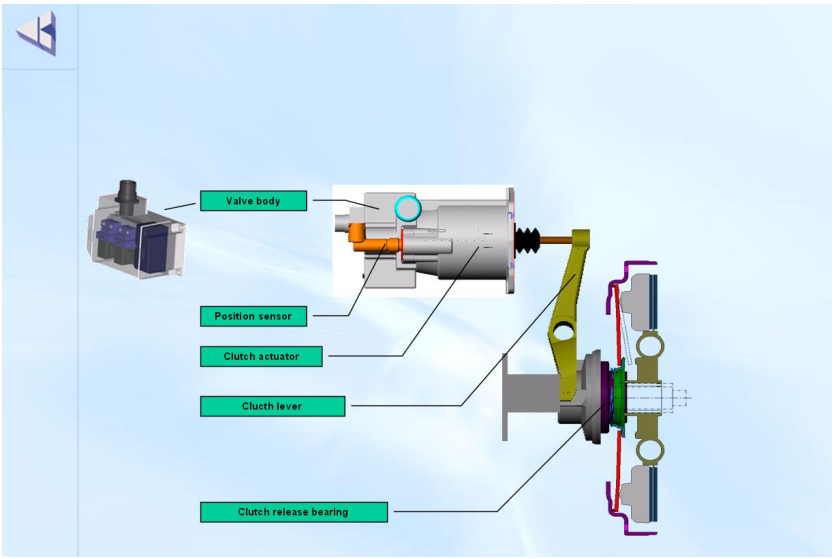

Figure 1.1: Clutch actuator system, courtesy of Kongsberg Automotive.

The actuator is not concentric as the one investigated by Kaasa [6]. This enables the actuator to be replaced without dismounting the transmission, which saves repair time.

The air flow in and out of the high pressure chamber is controlled by two on-off valves. The supply valve is connected to the vehicle's pneumatic system and the larger exhaust valve is connected to the atmosphere. The low pressure chamber is connected to the atmosphere through an opening in the cylinder chamber. Pulse-width-modulation (PWM) is used to control the valves. A spring is mounted onto the piston rod to provide a permanent force acting on the release bearing of the clutch. This spring force is not important in the mathematical modeling of the system and its dynamics will be incorporated in the model of the clutch spring. A lip seal is used to minimize the air flow between the piston and the cylinder wall.

The position of the clutch actuator is measured by a position sensor. This is the only variable that is going to be measured when installed in a vehicle, caused by the extra cost of more sensors.

The variable of most interest is the actuator velocity. The actuator position measurement are contaminated with noise, therefore it is not desirable to just differentiate it to get the velocity. An alternative is to design an observer that imitates the plant's behavior and gets estimates of the variables of interest with less noise. Another benefit of an observer is that is possible to get estimates of other non-measured variables, thus justifying the choice of using position measurements only.

Robustness is a critical issue in applications with long lifetime and high profit loss when out

of operation. Therefore the clutch position controllers have to be robust with reference to parameter changes, as a result of environment or wear.

It is desirable to keep the models and equation solvers as simple as possible, because the computational power on the truck is limited. Therefore it will be attempted to use the Euler method (ODE1). This method is claimed to be the only reliable for solving discontinuous dynamics [11], although not mentioned in [17].

1.3 Current clutch control solutions

Until now, various controllers have been developed. The first work on the field for Kongsberg Automotive was done by Kaasa [6]. He developed two backstepping controllers, one exact and one approximate. The controllers showed high tracking performance. The observers utilized where based on output injection from the position measurement and open loop estimation of the less important states.

Non-adaptive backstepping controllers, with and without integral action, have been created [15]. These controllers did not handle unmodeled dynamics well and their performance was not satisfactory. In addition, an adaptive controller was developed. It performed well, but unmodeled dynamics increased the system response time.

Recently a boundary layer sliding mode controller have been applied to the clutch system [4], which yielded interesting results. Sliding mode controllers are robust against unmodeled dynamics, which will be the case for the clutch actuator where complex friction phenomena are present.

A proportional-derivative (PD) controller have shown promising performance, and will be used as a benchmark for the controllers in this report.

This report continues the work by discussing sliding mode and PD controller robustness, and applies a variable boundary layer sliding mode controller, which has not been done before, on the clutch system at Kongsberg Automotive. Also, a presentation of the results of application of a robust differentiator together with a controller is given.

Chapter 2

Simulation model

In order to test controller performance without having the test laboratory or truck at Kongsberg Automotive available, a simulation model has to be developed. The simulation model has to be more accurate than the control model given in Section 4.1, otherwise simulations could show trivial dynamics due to cancellation of system dynamics. The simulation model that will be used is found in [6]. This model contains pressure and temperature simulation of both chambers of the clutch actuator shown in Figure 2.1. All parameters used in the simulation model are shown in Table A.1 and A.2.

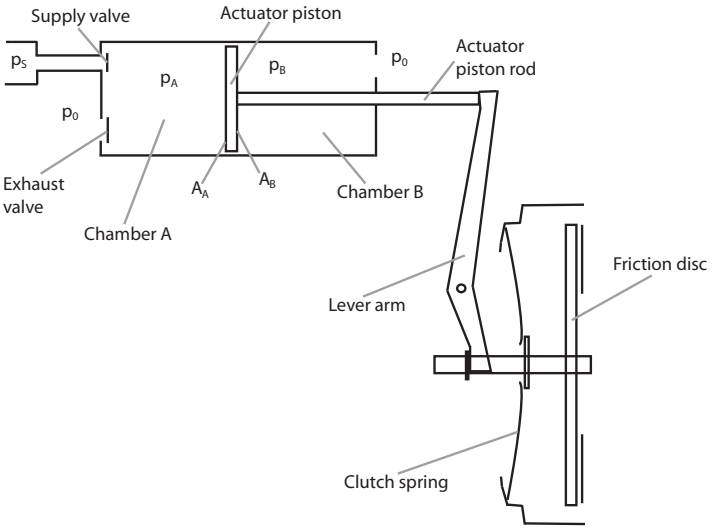

Figure 2.1: Schematic drawing of clutch and actuator system.

2.1 Motion dynamics model

The clutch motion dynamics is described by [6]

$$M\ddot{y} = A_0 P_0 + A_A p_A - A_B p_B - f_l(y) - f_f(\cdot) - f_h(y, v) \tag{2.1}$$

where y is the piston position, A_A, A_B and p_A, p_B are the area of the piston and pressure in chamber A and B respectively. $A_0 = A_B - A_A$ is the area of the chamber B side that is subjected to the atmospheric pressure P_0. Dynamic friction force is represented by f_f, f_l is the force exerted by the clutch spring and f_h is the hard stop force that simulates the actuator chamber wall and the clutch plate. M is the mass of the moving parts of the actuator.

The equation for the clutch motion (2.1) can be rewritten by using the variables q_A and q_B introduced in Section 2.2

$$\ddot{y} = \frac{1}{M}\left(\frac{A_A}{V_A(y)}q_A - \frac{A_B}{V_B(y)}q_B + AP_0 - f_l(y) - f_f(\,\cdot\,) - f_h(y,v)\right) \tag{2.2}$$

2.1.1 Friction model

The friction in the actuator is in [6] modeled as simplification of the LuGre friction model which is explained in [3]. The friction force is given by

$$f_f(v,z) = D_v v + K_z z + D_{\dot{z}}\dot{z}(v,z) \tag{2.3}$$

where D_v is viscous friction, K_z and $D_{\dot{z}}$ are deflection stiffness and damping. The pre-sliding dynamics are modeled by

$$\dot{z} = v - \frac{K_z}{F_C}|v|_s z \tag{2.4}$$

where z is the deflection variable and $|v|_s$ is a smooth absolute value function given by

$$|v|_s = \sqrt{v^2 + \epsilon_0^2} \tag{2.5}$$

where $\epsilon_0 > 0$ is a small tunable parameter. The smooth absolute value function is used to avoid numerical problems when the speed is close to zero.

2.1.2 Hardstop force

The mechanical constraints on the clutch and actuator system is modeled by using a smooth dead zone function and a smooth indicator function [6], which enables a spring-damper system when the constraints are active. The hardstop force is given by

$$f_h(y,v) = K_h\mu_h(y) + D_h v\rho_h(y) \tag{2.6}$$

where K_h and D_h are spring stiffness and damping coefficient respectively. The smooth dead zone function are given by

$$\mu_h(y) = \epsilon_h g\left(\frac{y - y_{ub}}{\epsilon_h}\right) - \epsilon_h g\left(\frac{y_{lb} - y}{\epsilon_h}\right) \tag{2.7}$$

where $g(\,\cdot\,)$ is a smooth is a smooth plus function constructed by a spline function given by

$$g(x) = \begin{cases} x, & x > 1 \\ \frac{3}{16} + \frac{1}{2}x + \frac{3}{8}x^2 - \frac{1}{16}x^4, & |x| \le 1 \\ 0, & x < -1 \end{cases} \tag{2.8}$$

which gives a smooth transition from a horizontal line to a line with unity slope. The σ_h determines the width of the transition, and y_{lb} and y_{ub} gives the lower and upper bound.

The smooth indicator function $\rho_h(y)$ is given by

$$\rho_h(y) = h\left(\frac{y - y_{ub}}{\epsilon_h}\right) + h\left(\frac{y_{lb} - y}{\epsilon_h}\right) \tag{2.9}$$

where the smooth step function gives a smooth transition from a horizontal line at $y = 0$ to a horizontal line at $y = 1$, given by the spline function

$$h(x) = \begin{cases} 1, & x > 1 \\ \frac{1}{2} + \frac{15}{16}x - \frac{5}{8}x^3 + \frac{3}{16}x^5, & |x| < 1 \\ 0, & x < -1 \end{cases} \tag{2.10}$$

Suitable values for ϵ_h, y_{lb}, y_{ub}, K_h and D_h are found by trial and error. It is important that the clutch in the simulation model stops with a non-oscillatory motion at the same position as the real clutch. Therefore y_{ub} is the least important parameter. Suitable values are given in Table 2.1.

Table 2.1: Hardstop force model parameters

Parameter	Value	Description
ϵ_h	$5 \cdot 10^{-4}$ m	Smoothing width
y_{lb}	$-\frac{\epsilon_h}{2} = -2.5 \cdot 10^{-4}$ m	Lower break point
y_{ub}	0.025 m	Upper break point
K_h	$3 \cdot 10^7$ N/m	Hardstop spring stiffness
D_h	$1 \cdot 10^3$ Ns/m	Hardstop damping coefficient

This values will restrict the clutch position to a lower bound of around $y = 0$ mm and an upper bound around $y = 25$ mm, as will be similar to the limits of a new clutch. Obviously, the friction disc of a worn clutch will be thinner, allowing the clutch to move to a position lower than $y = 0$ mm.

2.1.3 Clutch spring force model

The clutch load force $f_l(y)$ is given by [9]

$$f_l(y) = \theta_l^T \phi_l(y) \tag{2.11}$$

where θ_l is a vector of weighting parameters and ϕ_l is a vector of basis functions. The basis functions are B-splines, defined by

$$\phi_{l1} = \begin{cases} 0, & y < t_1 \\ y - t_1, & t_1 \leq y < t_2 \\ -76.92308y^2 + 1.3077y - 3.0769 \cdot 10^{-4}, & t_2 \leq y < t_3 \\ -76.92308t_3^2 + 1.3077t_3 - 3.0769 \cdot 10^{-4}, & y > t_3 \end{cases} \tag{2.12}$$

$$\phi_{l2} = \begin{cases} 0, & y < t_2 \\ 7.6923 \cdot 10^{-2} y^2 - 3.0769 \cdot 10^{-4} y - 3.0769 \cdot 10^{-7}, & t_2 \leq y < t_3 \\ y - 8.4968 \cdot 10^{-3}, & y > t_3 \end{cases} \tag{2.13}$$

$$\phi_{l3} = \begin{cases} 0, \quad y < t_2 \\ -2.3327 \cdot 10^3 y^3 + 47.2372 y^2 - 0.1610 y - 1.5163 \cdot 10^{-4}, & t_2 \leq y < t_4 \\ 2.3327 \cdot 10^3 y^3 - 113.7192 y^2 + 1.6900 y - 6.9439 \cdot 10^{-3}, & t_4 \leq y < t_5 \\ 0, & y \geq t_5 \end{cases} \tag{2.14}$$

where $t = [0\ 2\ 8.5\ 11.5]$ mm and $t_5 = 2t_4 - t_2$. The weighting parameter vector is chosen in [9] to be $\boldsymbol{\theta}_l = [8.2850 \cdot 10^5, -0.1834 \cdot 10^5, 6.1399 \cdot 10^5]$.

The clutch spring model force are shown in Figure 2.2.

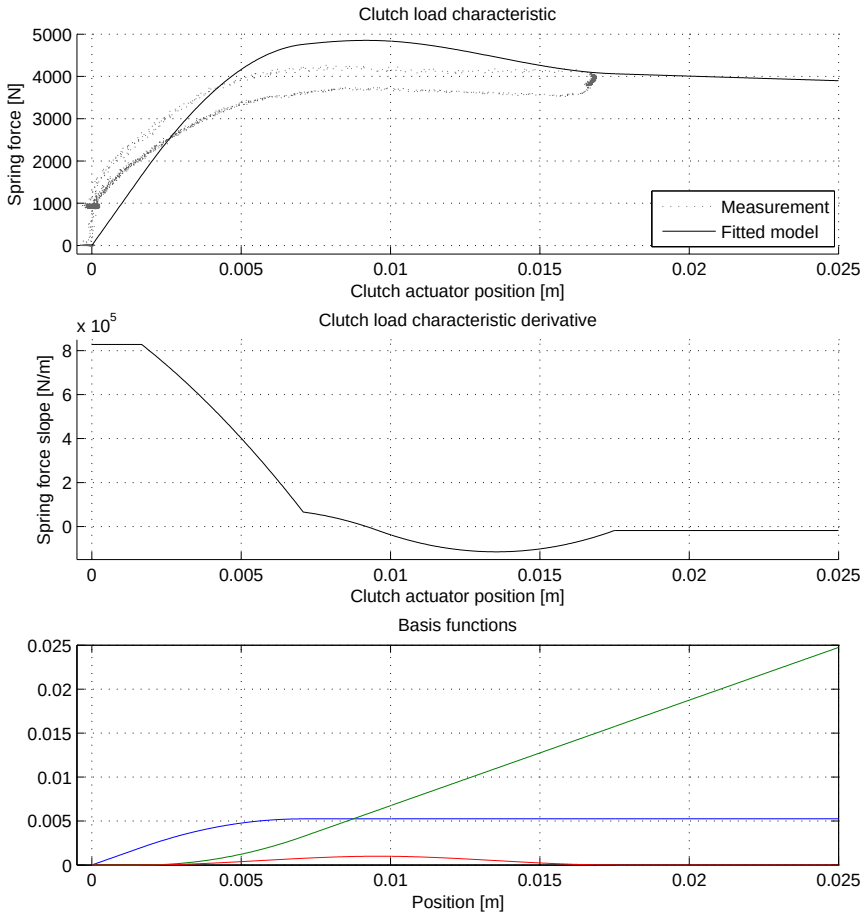

Figure 2.2: Clutch spring force model.

These clutch spring force model parameters corresponds to a new clutch. A worn clutch spring will exhibit a different force profile. A profile of a worn clutch is shown in [6], but there the

actuator system has a different layout[1] yielding a different force, possibly with the same profile shape only multiplied with a constant caused by the lever arm.

2.2 Air dynamics model

2.2.1 Chamber A

Chamber A is described by [6]

$$\dot{p}_A = -\frac{\kappa A_A v}{V_A(y)} p_A + \frac{\kappa R T_{in,A}}{V_A(y)} w_{in,A} - \frac{\kappa R T_A}{V_A(y)} w_{out_A} + \frac{(\kappa-1) H_w A_{w,A}(y)}{V_A(y)} (T_w - T_A) \tag{2.15}$$

$$\begin{aligned} \dot{T}_A = &-\frac{(\kappa-1) A_A v}{V_A(y)} T_A + \frac{(\kappa T_{in,A} - T_A) R T_A}{p_A V_A(y)} w_{in,A} - \frac{(\kappa-1) R T_A^2}{p_A V_A(y)} w_{out,A} \\ &+ \frac{(\kappa-1) T_A H_w A_{w,A}(y)}{p_A V_A(y)} (T_w - T_A) \end{aligned} \tag{2.16}$$

where and p_A and T_A are the pressure and temperature of chamber A respectively, κ is the ratio of specific heats, R is the gas constant for air, H_w is the empirical heat coefficient for the actuator cylinder wall, T_w is the wall temperature(assumed constant). The chamber A volume is given by

$$V_A = V_{A0} + A_A y \tag{2.17}$$

The effective area of the wall of heat transfer is given by

$$A_{w,A}(y) = A_{wA,0} + L_{wy} \tag{2.18}$$

where $A_{wA,0}$ is the area of heat transfer at $y = 0$, and L_{wy} is the inner perimeter of the actuator cylinder wall.

For numerical reasons the above equations can be rewritten by the use of a new variable $q_A = p_A V_A(y)$, which will be a measure of the amount of air inside the actuator chamber.

Differentiation gives

$$\dot{q}_A = \frac{dV_a(y)}{dt} p_A + V_A(y) \dot{p}_A$$

The q_A and temperature dynamics are now given by

$$\dot{q}_A = \frac{(1-\kappa) A_A v}{V_A(y)} q_A + \kappa R T_{in,A} w_{in,A} - \kappa R T_A w_{out,A} + (\kappa-1) H_w A_{w,A}(y)(T_w - T_A) \tag{2.19}$$

$$\begin{aligned} \dot{T}_A = &-\frac{(\kappa-1) A_A v}{V_A(y)} T_A + \frac{(\kappa T_{in,A} - T_A) R T_A}{q_A} w_{in,A} - \frac{(\kappa-1) R T_A^2}{q_A} w_{out,A} \\ &+ \frac{(\kappa-1) T_A H_w A_{w,A}(y)}{q_A} (T_w - T_A) \end{aligned} \tag{2.20}$$

[1] The clutch actuator in [6] is concentric, but here the actuator is mounted outside the clutch housing, acting on the clutch via a lever arm.

2.2.2 Chamber B

The corresponding equations for chamber B are found in [6]

$$\dot{p}_B = \frac{\kappa A_B v}{V_B(y)} p_B + \frac{\kappa R T_{in,B}}{V_B(y)} w_{in,B} - \frac{\kappa R T_B}{V_B(y)} w_{out,B} + \frac{(\kappa-1) H_w A_{w,B}(y)}{V_B(y)} (T_w - T_B) \tag{2.21}$$

$$\begin{aligned} \dot{T}_B = {} & \frac{(\kappa-1) A_B v}{V_B(y)} T_B + \frac{(\kappa T_{in,B} - T_B) R T_B}{p_B V_B(y)} w_{in,B} - \frac{(\kappa-1) R T_B^2}{p_B V_B(y)} w_{out,B} \\ & + \frac{(\kappa-1) T_B H_w A_{w,B}(y)}{p_B V_B(y)} (T_w - T_B) \end{aligned} \tag{2.22}$$

where the volume of chamber B is given by

$$V_B = V_{B0} - A_B y \tag{2.23}$$

The effective area of the wall of heat transfer is given by

$$A_{w,B}(y) = A_{wB,0} - L_{wy} \tag{2.24}$$

The equations for chamber B can be rewritten in the same fashion as the equations for chamber A. Using $q_B = V_B(y) p_B$ yields

$$\dot{q}_B = \frac{(\kappa-1) A_B v}{V_B(y)} q_B + \kappa R T_{in,B} w_{in,B} - \kappa R T_B w_{out,B} + (\kappa-1) H_w A_{w,B}(y)(T_w - T_B) \tag{2.25}$$

$$\begin{aligned} \dot{T}_B = {} & \frac{(\kappa-1) A_B v}{V_B(y)} T_B + \frac{(\kappa T_{in,B} - T_B) R T_B}{q_B} w_{in,B} - \frac{(\kappa-1) R T_B^2}{q_B} w_{out,B} \\ & + \frac{(\kappa-1) T_B H_w A_{w,B}(y)}{q_B} (T_w - T_B) \end{aligned} \tag{2.26}$$

2.3 Flow modeling

2.3.1 Flow simulation model

The simulation model of the flow through the control valves is taken from [6]

$$w = \rho_0 \sqrt{T_0} C \cdot \omega_e \left(\frac{p_l}{p_h} \right) \frac{p_h}{\sqrt{T_h}} u \tag{2.27}$$

where the pressure ratio function is given by

$$\omega_e = \sqrt{1 - r^2} \tag{2.28}$$

where the pressure ratio is given by $r = \frac{p_l}{p_h}$, where p_l is the pressure at the low pressure side and p_h is the pressure at the high pressure side. C is chosen to correspond to the valves, for chamber A, and orifice for chamber B. The control input $u \in [0, 1]$ is the valve opening. All coefficients are given in Appendix A.

The control system will run at a time step of 0.001 s and the pulse period is 0.01 s, which means that the control valve resolution will be 0.1.

The valves are modeled as they have a opening that is equal to the duty cycle for the whole PWM period, but in reality they will open fully for the duration of the duty cycle and close for the rest of the PWM period.

2.3.2 Valve dead zone

The valves need about 0.0007 s to open or close. This means that they will not open with a duty cycle below 0.07 at PWM frequency 100 Hz, as well as introducing a time delay of 0.0007 s when the valve dynamics are neglected. The time delay will not be implemented in the simulation model.

2.4 Measurement noise

To test a complete control system, measurement noise has to be simulated. With the assumption that the noise is white, the clutch position measurement is found to have variance $8.4542 \cdot 10^{-9}$ m^2 and mean $-2.0835 \cdot 10^{-5}$ m when the clutch is at rest. By assuming that the mean value of the position measurement is the actual clutch position, the measurement noise can be simulated by white noise with the same variance.

Even when the real clutch is placed at $y = 0$ and the supply valve is not opened, the clutch may be moving because of vibrations from the engine, making it difficult to identify the real motion and measurement noise.

The measurement signal may also include dead signal, i.e. points where the measurement signal is lost, and wild-points, i.e. single points whose values are obviously wrong. These effects will not be included in the simulation model.

2.5 Verification of the simulation model

To test the simulation model, control input is applied to the simulation model and the output is compared to measurements from the test laboratory. Simulation results without artificial measurement noise are shown in Figure 2.4 - 2.7. Figure 2.3 shows the input applied to the real system and the simulation model.

It can be seen that the simulation model behaves similar to the real clutch, although the clutch position deviates only slightly during transients, but the stationary error is quite large. The response of the actuator is faster in the simulation model. These errors is believed to stem from the friction and spring model, but also disturbances in the test setup can be the source of some of the errors. The neglected valve dynamics may also play a role. The real system has

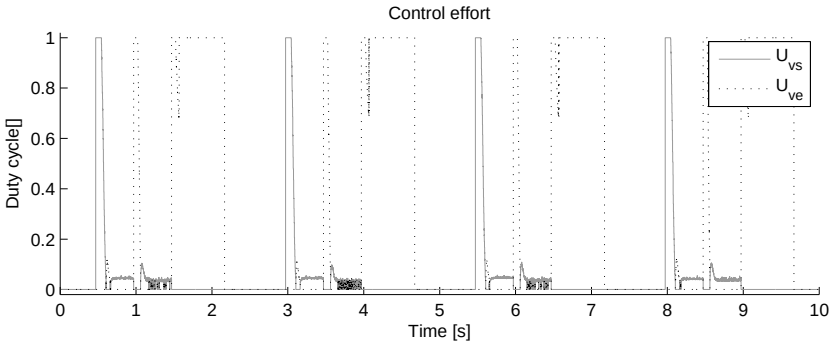

Figure 2.3: Control effort given by the duty cycle. ODE3, time step 0.001 s.

a time delay when the valves are opened, which is caused by the rubber tubing[2] that connect the valve housing to the actuator chamber; the PWM-cycles in the simulation model and in the real truck are not synchronized.

The velocity and acceleration plots show that the simulation model covers the main dynamics of the real system.

The pressure from the simulation model and measurement differs. It seems that the pressure in the simulation model tends to overshoot, and the response is too quick which may be caused by the transport delay in the tube.

The non-measured states seem to be reasonable. The temperature inside the chambers rise drastically together with pressure, as air is let into it. When the piston is held at rest away from starting point, the temperature is changed and heat is transferred from or to the cylinder walls, such that temperature approaches the environmental temperature of $293\,\mathrm{K} \approx 20°\mathrm{C}$. The flow into chamber A is shaped like round stairs due to PWM controlled valves, unless the control input equals 1 (or 0).

The pressure of chamber B is around the environmental pressure, which seems reasonable since the chamber is connected to the environment via a duct. During transients, the pressure increases slightly causing the temperature to rise and heat to flow from the air to the cylinder wall, and opposite when the piston is moved towards $y = 0\,\mathrm{mm}$. The flow in chamber B is closely related to the velocity of the piston, and the compressibility of air causes the flow to be smooth.

[2] In the truck the prototype valves are mounted in a housing that is connected to the actuator chamber with a rubber tubing that has a length of approximately 30 cm. The differences between the real system and the simulation model regarding the tube are commented in Section 5.3.1.

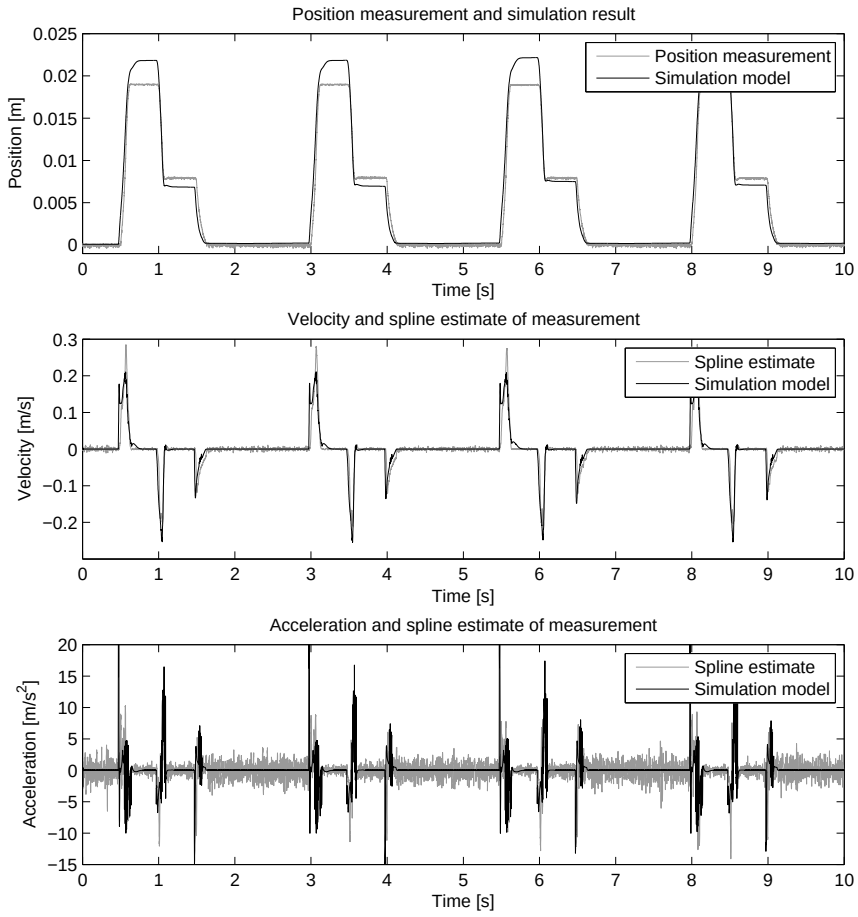

Figure 2.4: Simulation model test. Position, velocity and acceleration simulation results, position measurement and spline estimate. ODE3, step size 0.001 s.

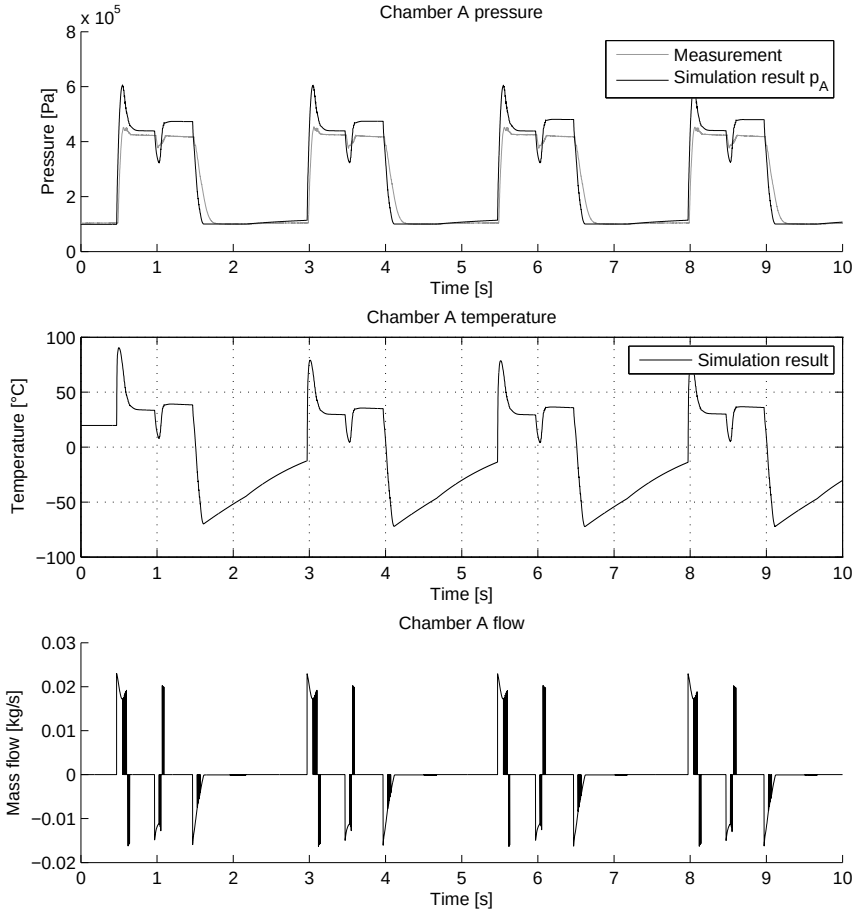

Figure 2.5: Chamber A pressure, temperature and flow. ODE3, step size 0.001 s.

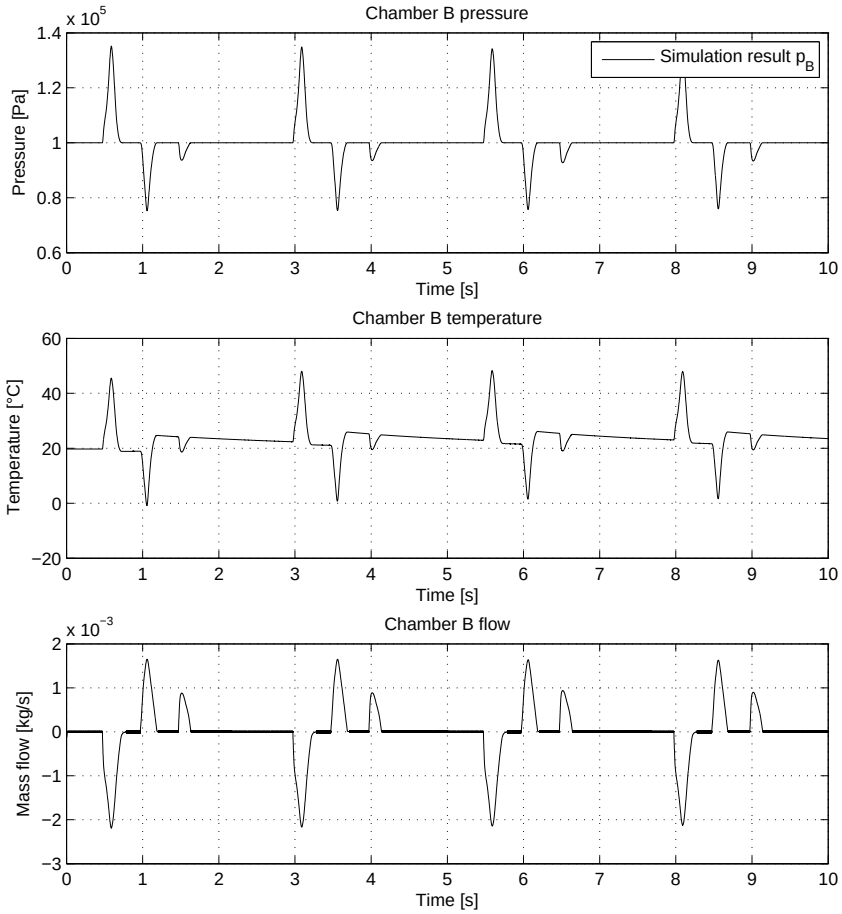

Figure 2.6: Chamber B pressure, temperature and flow. ODE3, step size 0.001 s.

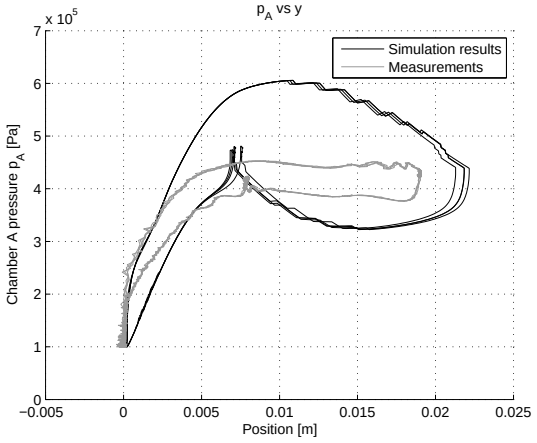

Figure 2.7: Simulation model test, position versus chamber A pressure. ODE3, step size 0.001 s.

Chapter 3

Measurement filter

Various approaches to the problem of obtaining good state estimates from the clutch position measurement have been made [6], [8] and [18]. Mostly Lyapunov theory have been used in the observer design.

In this chapter a measurement filter will be designed using the robust differentiation technique of Levant [13], which is inspired by higher order sliding mode control. It will be compared to a linear first order filter. In general a linear low pass filter will output smoother estimates compared to a robust differentiator, but it will suffer from phase lag [5]. The reason for choosing a first order filter for comparison is that is simple to understand and make decisions with reference to accuracy and smoothness.

The position measurement is assumed to be good enough for direct application in the controller and the necessary components of the control system. Filters have to be utilized to get estimates of the clutch velocity and acceleration, which is necessary for the calculation of the sliding surfaces in the sliding mode controllers and the pressure estimate for all controllers. The PD controller designed in Section 4.6 only needs position measurement, because the limited derivative action will take care of filtering and differentiation itself.

Differentiation of noisy signals is not straightforward. This problems are handled by an observer, robust differentiator or filter and by the controller to a certain degree.

3.1 Linear filter

The linear filter is supposed to filter and differentiate the position measurement signal. The transfer function of the filter is written as a first order filter with time constant T in series with a differentiation operator, i.e. a zero at the imaginary axis

$$h_f(s) = \frac{s}{1+Ts} \tag{3.1}$$

By combining the filtering and differentiation in one single operation ensures that implementation is possible, because the transfer function is proper.

The filter will be written in state space form to be applicable to the real system. The realization is made by following the algorithm in [2], and is shown in detail in Appendix B.1. It is given by

$$\dot{x} = -\frac{1}{T}x + u \tag{3.2}$$

$$y = -\frac{1}{T^2}x + \frac{1}{T}u \tag{3.3}$$

where y is the filtered derivative of the filter input u.

The low pass filter implementation is shown in Figure D.4.

3.2 Robust differentiation

Levant [13] proposes the following robust differentiator

$$\dot{z}_0 = v_0, v_0 = -\lambda_k L(t)^{1/(k+1)} \left|z_0 - f(t)\right|^{k/(k+1)} \operatorname{sign}(z_0 - f(t)) + z_1 \tag{3.4}$$

$$\dot{z}_1 = v_1, v_1 = -\lambda_{k-1} L(t)^{1/(k)} \left|z_1 - v_0)\right|^{k/(k+1)} \operatorname{sign}(z_1 - v_0) + z_2 \tag{3.5}$$

$$\vdots \tag{3.6}$$

$$\dot{z}_{k-1} = v_{k-1}, v_{k-1} = -\lambda_1 L(t)^{1/2} \left|z_{k-1} - v_{k-2})\right|^{1/2} \operatorname{sign}(z_{k-1} - v_{k-2}) + z_k \tag{3.7}$$

$$\dot{z}_k = -\lambda_0 L(t) \operatorname{sign}(z_k - v_{k-1}) \tag{3.8}$$

where the input signal is $f(t)$ and its kth derivative is z_k. Parameters $\lambda_0, \lambda_1, \ldots, \lambda_k$ are chosen such that the differentiator is finite-time stable[1] with $L \equiv 1$. It is assumed that the kth derivative has a know local time varying Lipschitz constant[2] $L(t) > 0$.

Levant [13] proposes the following parameters $\lambda_0 = 1.1$, $\lambda_1 = 1.5$, $\lambda_2 = 2$, $\lambda_3 = 3$, $\lambda_4 = 5$ and $\lambda_5 = 8$, for $k \leq 5$.

The sign of the slope of the highest derivative, $\dot{z}_k$, is determined by the sign of the difference between the highest derivative z_k and the slope of the estimate of the second highest derivative v_{k-1}. The steepness of z_k is determined by a scaled norm of a vector consisting of the input signal and its derivatives up to the kth derivative and a estimate of the Lipschitz constant for $\dot{z}_k$.

The robust differentiator can be compared to a higher order sliding mode controller, here illustrated by the order two, where the sliding surface is given by

$$\sigma = z_0 - f(t) = 0 \tag{3.9}$$

The control law is constructed by using an auxiliary equation

$$\dot{x} = u \tag{3.10}$$

[1] There exists such functions $\delta(t) > 0$ and $T(t) > 0$ that any solution of (3.4) satisfying conditions $|z_i(t_0) - f_0^{(i)}(t_0)| \leq \delta(t_0)$, satisfies $z_i = f_0^{(i)}(t)$, $i = 0, \ldots k$, for any $t \geq t_0 + T(t_0)$. Theorem 1 [13].

[2] The Lipschitz constant L is given by $||f(t,x) - f(t,y)|| \leq L||x - y||, \forall (t,x), (t,y)$ in some neighborhood of the starting condition (t_0, x_0) [7].

as described in [10]. The control law is described by

$$u = u_1 - \lambda |x - f(t)|^{1/2} \operatorname{sign}(x - f(t)) \tag{3.11}$$

$$u_1 = -\alpha \operatorname{sign}(x - f(t)) \tag{3.12}$$

where $\alpha, \lambda > 0$. According to (3.10), u is the output of the differentiator. The principle can be extended to an arbitrary differentiator order.

The robust differentiator is shown in Figure D.2. Derivatives for $L(t)$ are obtained using the derivative[3] block in Simulink, as shown in Figure D.3.

A deeper investigation on the use of Levant robust differentiator as an observer for the clutch system, the effect of solver step size and solver algorithm is found in [5].

3.3 Filter testing

In this section both filters will be tested on measurements from the test lab at Kongsberg Automotive and the simulation model in Chapter 2. A simulation test with the robust differentiator in a feedback loop can be found in Section 5.2.7.

The filter parameters has been set by the use of common sense and may have to be adjusted to work with the controllers.

3.3.1 Measurement filter test

Position measurement from the test lab at Kongsberg Automotive will in this section be put into the robust differentiator and the low pass filter. The measurements are taken using a controller to track a repetitive reference, therefore only a segment of the test results is shown in the figures. The results are shown in Figure 3.1 - 3.3. The robust differentiator parameter is given by $L(t) = 4\sqrt{y^2 + \dot{y}^2 + \ddot{y}^2 + 10}$, which is shown in Figure C.1, and the time constant of the filter is set to $T = 1 \cdot 10^{-2}$ s for the velocity filter and for the acceleration filter. All results are obtained with ODE1 (Euler method) with step size 0.001 s.

It can be seen that the response in the velocity estimate is fast, but the estimate oscillates as a result of measurement noise. If the parameters are changed such that $L(t)$ becomes smaller, the estimates will be less affected by noise but the transient performance will be significantly worse. Large overshoots in the estimates are observed, because the time needed to correct the estimates is long due to the low value of $L(t)$ when the input is constant.

The response in the acceleration estimate is slower and the influence of the noise is significant.

The output of the low pass (LP) filter is smooth and suffer from phase lag[4] as expected. An advantage of the LP filter is that it is straightforward to adjust the output smoothness and accuracy.

[3] The derivative block outputs the difference between the present and previous input, divided by the step size. This method will introduce a small delay, because the output of the block will be an approximation of the derivative of the input at the mid point of the time step.

[4] The phase lag of a linear first order low pass filter is proportional to the time constant T of the filter.

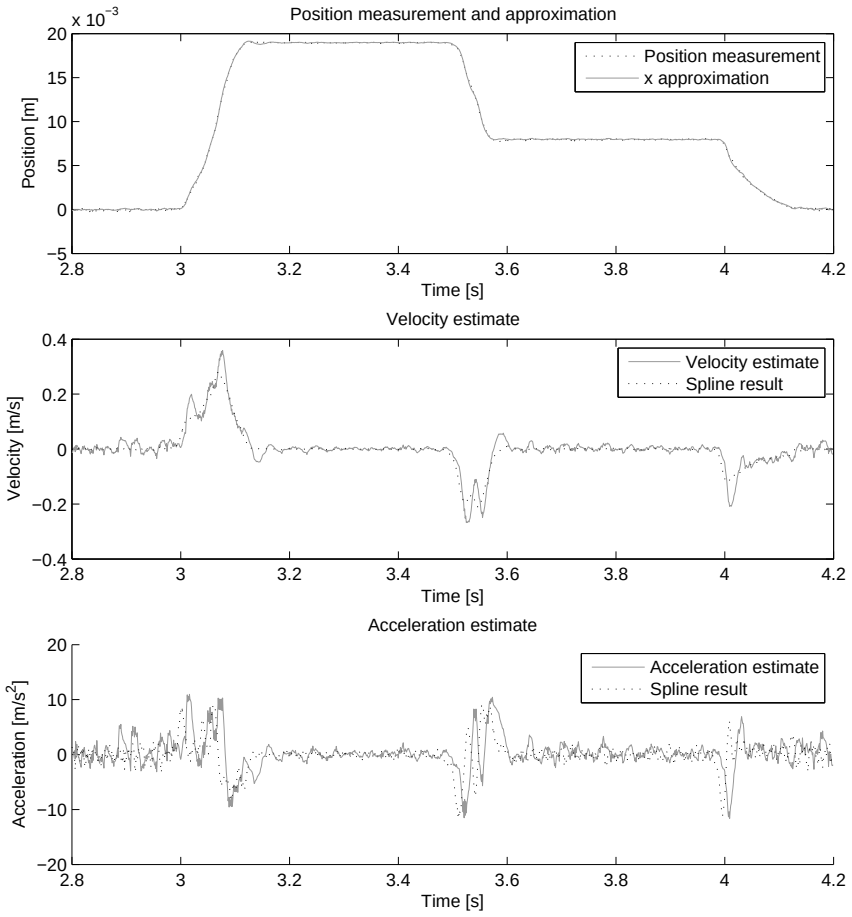

Figure 3.1: Position, velocity and acceleration estimate from the robust differentiator (RD) compared to measurement and spline estimates. ODE1, step size 0.001 s.

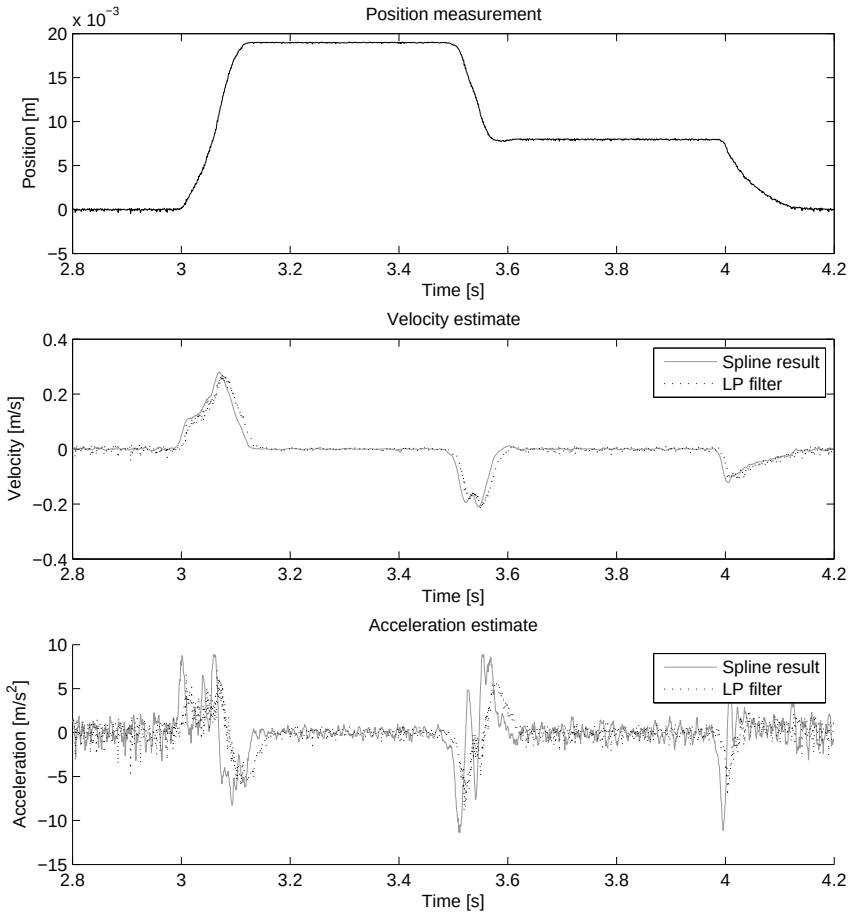

Figure 3.2: Position, velocity and acceleration estimate from the low pass (LP) filter compared to measurement and spline estimates. ODE1, step size 0.001 s.

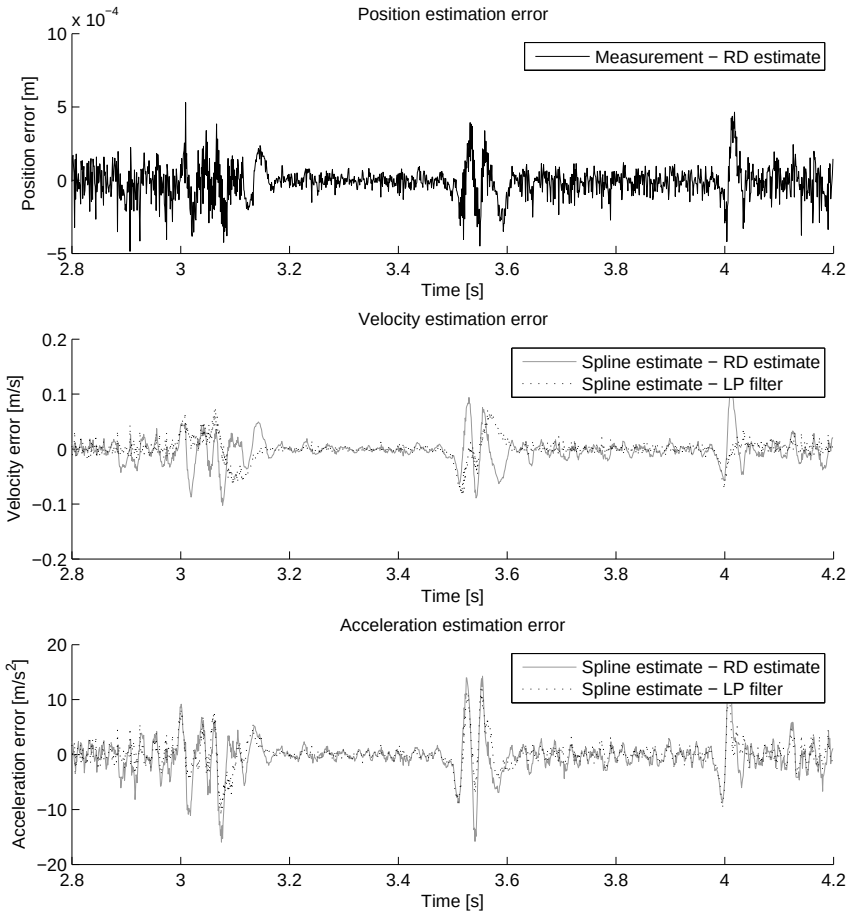

Figure 3.3: Deviation from the measurement and spline estimate for the robust differentiator and low pass filter. ODE1, step size 0.001 s.

3.3.2 Simulation model filter test

In this section simulation results obtained from the simulation model are filtered using the LP filter and the robust differentiator. The input applied equals the input used in the measurements from Kongsberg Automotive. Measurement noise is enabled and the filter parameters are kept unchanged.

Figure 3.4 - 3.6 show filter estimates of position, velocity and acceleration, compared to simulation state values without noise. The corresponding $L(t)$ is shown in Figure C.2.

Notice that both filters smooth out the real motion, which is clearly visible in the acceleration estimate. The acceleration is oscillatory.

The observations are equal to the result from the measurement test. The robust differentiator estimates are oscillatory and the LP filter estimates are smooth. The linear filter thus seem to be the best choice.

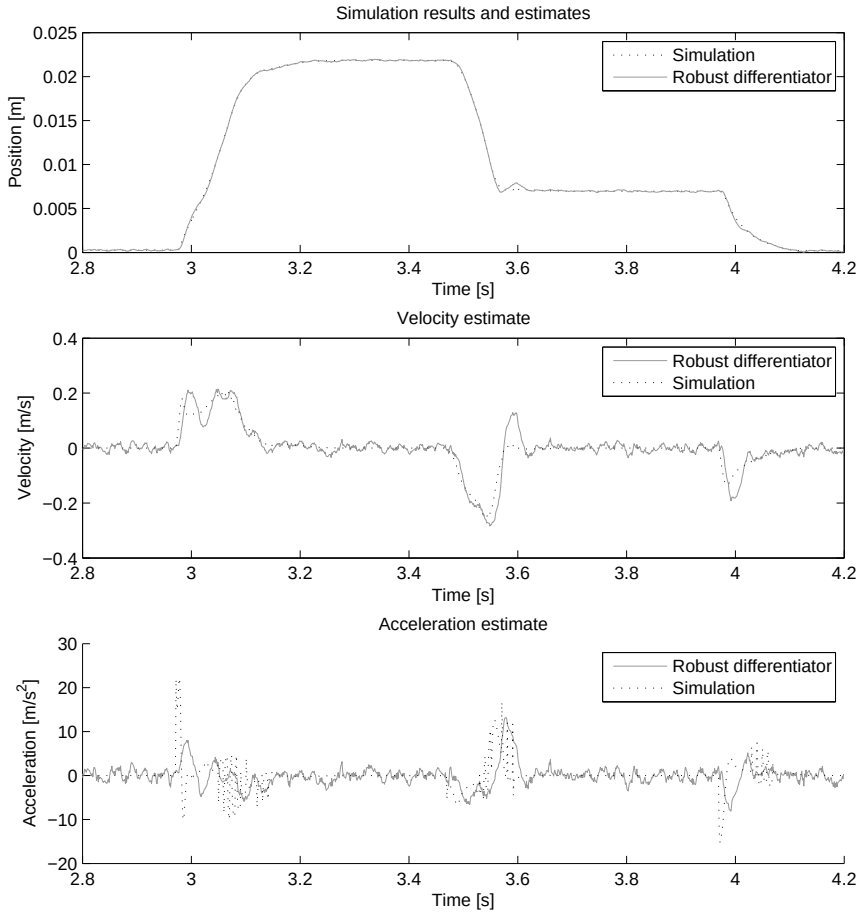

Figure 3.4: Position, velocity and acceleration estimate from the robust differentiator (RD) compared to simulation value. ODE1, step size 0.001 s.

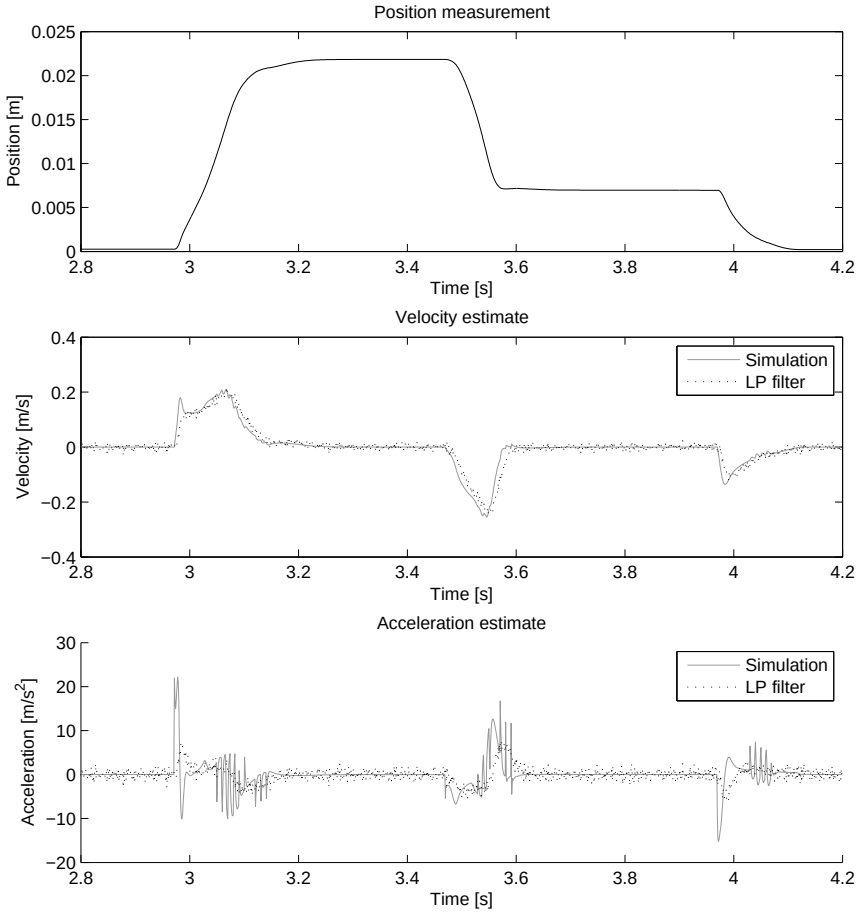

Figure 3.5: Position, velocity and acceleration estimate from the low pass (LP) filter simulation value. ODE1, step size 0.001 s.

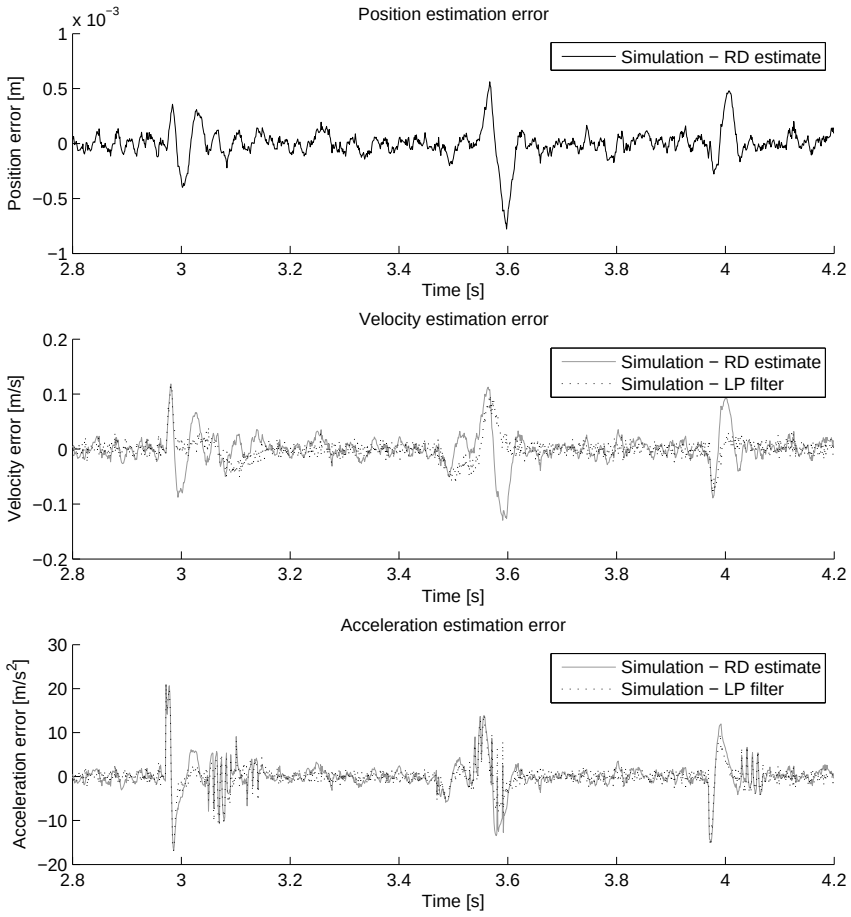

Figure 3.6: Deviation from the simulation values for the robust differentiator and low pass filter. ODE1, step size 0.001 s.

3.4 Conclusion on measurement filter

The above analysis show that the output of the low pass filter is smooth as opposed to the robust differentiator estimate which is oscillatory. Both filters have phase lag of approximately the same size for the tested parameters.

If it is important to minimize response time, the robust differentiator is favorable, but may introduce problems related to noise. It is difficult to adjust the parameters to get smoother estimates.

When smooth estimates are important and phase lag is not a large problem, a low pass filter would perform well. The adjustment of the parameter is straightforward and easy to understand.

With less measurement noise, the robust differentiator will produce better results, but in that case the low pass filter time constant may be lowered, such that the difference in quality of the estimates from the two filter will probably be small.

For use in feedback loops, the linear filter seem to be the best choice, because smooth estimates lead to smoother input, with that extend the lifetime of the system.

Chapter 4

Control design

In this chapter a proportional-derivative (PD) controller and sliding mode (SM) controllers will be developed for the clutch actuator system. The PD controller will be used to compare the robustness and performance of the SM controllers. It is expected that the PD controller will less able to track fast reference trajectories compared to SM control as mentioned in [6].

Because pulse-width modulation (PWM) is used to control the flow, non-smooth control input will not cause extra wear and tear on the control valves, as long it not varies between positive and negative values or not always open.

4.1 Control design model

A simplified version of the system dynamics are given by (9.6) in [6]

$$\dot{y} = v \tag{4.1}$$

$$\dot{v} = \frac{1}{M}\left(Ap - AP_0 - f_l(y) - D_v v\right) \tag{4.2}$$

$$\dot{p} = -\frac{A}{V(y)}vp + \frac{RT_0}{V(y)}u \tag{4.3}$$

where the flow into the actuator chamber is written as mass flow $w_v(p)$, and this is the input to the system $u = w_v(p)$.

Since the controller will output the desired flow, a translation from $w_v(p)$ to duty cycle has to be made. This is done in Section 4.3. The control model of the mass flow is given by

$$w_v(p) = \rho_0\sqrt{T_0}C \cdot \omega_e\left(\frac{p_l}{p_h}\right)\frac{p_h}{\sqrt{T_h}}\tilde{u} \tag{4.4}$$

where $\tilde{u}$ is the duty cycle of the valve. A simplification of the control input is performed. The input is assumed to be multiplied by the duty cycle, i.e. kept at the duty cycle value for the

entire pulse period, and not at one for the duty cycle length and completely shut for the rest of the period[1]. The duty cycle is given by $\tilde{u} \in [0, 1]$[2].

4.2 Reference trajectory

To get a smooth reference transition when the desired for the clutch position is changed, a reference trajectory filter has to be made. This is done in [6] by generating a linear system where the poles can be placed at $s = -\lambda_r$, which gives a critically damped (and stable) reference system. The reference state space model is given as a canonical form

$$\dot{\boldsymbol{z}}_r = \begin{bmatrix} 0 & & \\ \vdots & \boldsymbol{I}_{n-1} & \\ 0 & & \\ -m_0 & \dots & -m_{n-1} \end{bmatrix} \boldsymbol{z}_r + \begin{bmatrix} 0 \\ \vdots \\ 0 \\ 0 \\ m_0 \end{bmatrix} r \tag{4.5}$$

where $\boldsymbol{z}_r = \left[y_r, \dot{y}_r, \dots, y_r^{(n-1)} \right]^T$ is the reference position and its derivatives up to order $(n-1)$, and $\boldsymbol{I}_{n-1}$ is the $(n-1)$ identity matrix. The characteristic polynomial is given by

$$p_1 = \lambda^5 + \lambda^4 m_4 + \lambda^3 m_3 + \lambda^2 m_2 + \lambda m_1 + m_0 \tag{4.6}$$

The characteristic polynomial for a fifth order system with all poles at $\lambda = -a_0$ is given by

$$p_2 = (\lambda + a_0)^5 = \lambda^5 + 5\lambda^4 a_0 + 10\lambda^3 a_0^2 + 10\lambda^2 a_0^3 + 5\lambda a_0^4 + a_0^5 \tag{4.7}$$

By comparing (4.6) and (4.7), the coefficients necessary for placing all poles of the reference system (4.5) at $\lambda = -a_0$

$$\begin{aligned} m_0 &= a_0^5 \\ m_1 &= 5a_0^4 \\ m_2 &= 10a_0^3 \\ m_3 &= 10a_0^2 \\ m_4 &= 5a_0 \end{aligned} \tag{4.8}$$

In this report $a_0 = 70$, which yields a time constant of $\frac{5}{70}$ s[3].

[1] This is a simplification as well, since the valve dynamics are neglected.

[2] In practice a input below $\tilde{u} = 0.07$ does not have any effect on the system due to the dead zone of the valves. See Section 2.3.2.

[3] In [4], [6] and [15], a time constant of 0.1 s is used. Applied to the controllers in this report, it yields considerably smaller tracking errors. A simulation plot of the variable boundary layer controller from Section 4.7.4 is shown in Figure C.8. The reason for choosing time constant $\frac{5}{70}$ s, is that satisfactory tracking with this time constant have been obtained at Kongsberg Automotive.

4.3 Inverse valve flow model

To obtain the control input to the plant i.e. the duty cycle for the valves, an inverse flow model for the valves has to be obtained. The orifice flow equation is given by [6]

$$w_v = \rho_0 \sqrt{T_0} C \cdot \omega_e \left(\frac{p_l}{p_h} \right) \frac{p_h}{\sqrt{T_h}} \tilde{u} \tag{4.9}$$

where $u \in [0, 1]$ is the control input and C is the flow conductance of the valve. By inserting the desired flow w_d, assuming that $T_h = T_0$ and solving for u an inverted flow model is obtained

$$u = \frac{w_d}{\rho_0 C \omega_e(\frac{p_l}{p_h}) p_h} \tag{4.10}$$

The maximum flow through the valve is given by the denominator of this expression. Care must be taken to avoid division by zero. The control input has to be distributed to the supply and exhaust valve, avoiding that both valves are open simultaneously, which is simply done by controlling a switch in accordance with the sign of $w_d(p)$.

By assuming $w_e = 1$[4] and $P_S > 0$, the inverse flow model for the supply valve can be written as

$$u_s = \underset{[0,1]}{\text{sat}} \left\{ \frac{w_d}{\rho_0 C_{vs} p_s} \right\} \tag{4.11}$$

and the corresponding equation for the exhaust valve is given by

$$u_e = \underset{[0,1]}{\text{sat}} \left\{ \frac{-w_d}{\max \left\{ G_{min}, \rho_0 C_{ve} \sqrt{1 - \left| \frac{p_0}{p} \right| p} \right\}} \right\} \tag{4.12}$$

where $G_{min} > 0$ is a parameter that ensures that the divisor is greater than zero.

The control input can only be updated at the starting point of the PWM cycle, thus a choice has to be made on the control update strategy. It is assumed that just taking the current control input at the starting point of the PWM cycle will lead to poor control. Therefore a weighted average of the control input signals calculated during the last PWM cycle is taken.

Simulations indicate that a good choice is w = [4 3 2 1 1/2 1/4 1/8 1/16 1/32 1/64], where the current input has highest weighting and the previous inputs has descending weighs. It is intuitively right to let the newest information weight most.

4.4 Pressure estimate

The inverse valve model input is chamber A pressure p. A pressure sensor is not wanted, therefore p has to be estimated. An estimate of p is also required in the equivalent control

[4] The choice of $w_e = 1$ for the supply valve has been reported by Kongsberg Automotive to be adequate.

in the sliding mode controller in Section 4.7. The acceleration equation in the control design model (4.2) can be rewritten as

$$\hat{p} = \frac{1}{A}\left(M\hat{\ddot{y}} + D_v\hat{\dot{y}} + f_l(y)\right) + P_0 \tag{4.13}$$

The inverse flow model algorithm will fail if the pressure estimate falls below the atmospheric pressure $1 \cdot 10^5$ Pa, therefore pressure estimate is altered to ensure that the lowest estimate is at least equal to the atmospheric pressure

$$\hat{p} = \max\left\{P_0, \frac{1}{A}\left(M\hat{\ddot{y}} + D_v\hat{\dot{y}} + f_l(y)\right) + P_0\right\} \tag{4.14}$$

The pressure estimate is heavily dependent on the estimate of the clutch load $f_l(y)$ and that could raise robustness issues, because the clutch load spring will alter with the age of the clutch.

The pressure estimate from a simulation is shown in Figure 4.1, together with measured pressure and pressure from the simulation model.

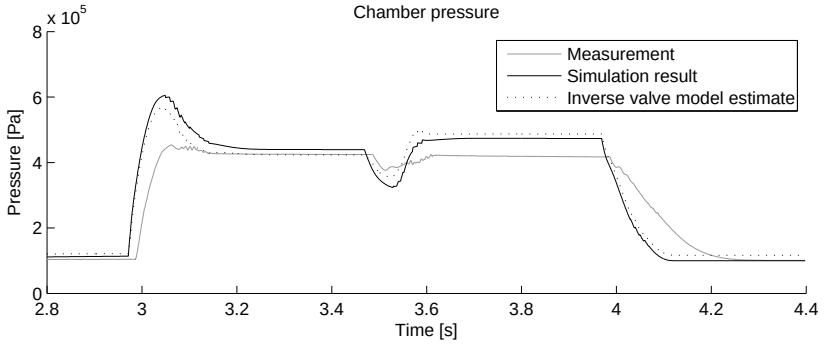

Figure 4.1: Pressure estimates from the simulation model and inverse valve model, and pressure measurement. ODE3, step size0.001 s.

It can be seen that the difference between the inverse valve model pressure and the simulation model pressure is significantly smaller than the deviation from the measurements. The inverse valve model pressure estimate seem to be satisfactory accurate for its use. Later the controllers will be tested with various changes on the pressure estimate parameters and with constant pressure as well.

The pressure estimate could be viewed as an observer together with the measurement filters, because they will output estimates of all the states in the control design model (4.1) - (4.3).

4.5 Controller disengage block

By normal driving, i.e. when the speed of the vehicle is over a certain value, such that clutch slip is not necessary for vehicle movement and no gear shift is performed, the clutch plates should be pressed together by the clutch spring such that the clutch is fully engaged. A

controller disengage block is positioned between the inverted valve model block and the clutch actuator model or real system. The controller disengage block[5] opens the exhaust valve for a specified time interval and then shuts both control valves. This is only performed when the clutch position and the desired clutch position and velocity are below pre-specified values, and is aborted when the condition no longer holds. This technique will increase the performance of the controllers and greatly reduce wear and tear of the clutch and actuator, as well as noise and energy usage.

It is important that the exhaust valve is not kept open too long, leading to low pressure inside the actuator chamber, resulting in slower response when the clutch plates is to be moved away from each other. If the exhaust valve is kept open to short, the air inside the actuator, which will cooled down as the pressure drop, may be heated by the actuator walls, resulting in pressure increase and the clutch plates may drift from each other.

The controller disengage block implementation is shown in Figure D.1.

4.6 PD controller

In this section a proportional-derivative (PD) controller will be developed. It will be based on linearization about an operating point $\boldsymbol{x}^* = [y^*, v^*, p^*]^T$, which is chosen to be around the point where the clutch slips, because it is critical that the model is accurate here. Another choice could be the mid-stroke of the actuator [6].

4.6.1 Operating point

According to [9], the point where the clutch slips is about $y \in [7, 8] \cdot 10^{-3}$ m. Therefore $\boldsymbol{x}^*$ is chosen where $y^* = 7.5 \cdot 10^{-3}$ m and $v^* = 0$ m/s, which inserted in (4.1)-(4.3), yields the following operating point

$$y^* = 7.5 \cdot 10^{-3} \text{ m} \tag{4.15}$$

$$v^* = 0 \text{ m/s} \tag{4.16}$$

$$p^* = 4.6495 \cdot 10^5 \text{ Pa} \tag{4.17}$$

the clutch load force at the given point is $f_l(y^*) = 4.4786 \cdot 10^5$ N, from the model in 2.1.3.

4.6.2 Linearization

The control design model (4.1)-(4.3) is going to be linearized about the operating point $\boldsymbol{x}^*$. To avoid stiff system dynamics, the control design model is scaled by using other measuring units for position and pressure. The system dynamics is rewritten with new scales on the state vector

$$\boldsymbol{x} = \begin{bmatrix} y \text{ [cm]} \\ v \text{ [m/s]} \\ p \text{ [bar]} \end{bmatrix} \tag{4.18}$$

[5] The controller disengage block is called Relax valves in [4].

The system equations now become

$$\dot{y} = 100v \tag{4.19}$$

$$\dot{v} = \frac{1}{M}\left(Ap \cdot 10^5 - AP_0 - f_l(0.01y) - D_v v\right) \tag{4.20}$$

$$\dot{p} = \frac{-A}{V(0.01y)}vp + \frac{RT_0}{V(0.01y)} \cdot 10^{-5}u \tag{4.21}$$

A general model of a control system is found in [2]

$$\dot{\boldsymbol{x}}(t) = \boldsymbol{h}(\boldsymbol{x}(t), \boldsymbol{u}(t), t) \tag{4.22}$$

$$\boldsymbol{y}(t) = \boldsymbol{f}(\boldsymbol{x}(t), \boldsymbol{u}(t), t) \tag{4.23}$$

and a linearization of this system, with a scalar input u, is given by

$$\dot{\boldsymbol{x}} = A\boldsymbol{x} + Bu \tag{4.24}$$

where

$$A = \frac{\partial \boldsymbol{h}}{\partial \boldsymbol{x}} = \begin{bmatrix} 0 & 100 & 0 \\ -\frac{1}{M}0.01 \cdot \frac{\partial f_l(y)}{\partial y}\Big|_{y^*} & -\frac{D_v}{M} & \frac{A}{M} \cdot 10^5 \\ \frac{-0.01A^2}{V(y^*)}v^*p^* & \frac{-A}{V(y^*)}p^* & -\frac{A}{V(y^*)}v^* \end{bmatrix} \tag{4.25}$$

and

$$B = \frac{\partial \boldsymbol{h}}{\partial u} = \begin{bmatrix} 0 \\ 0 \\ \frac{RT_0}{V(y^*)} \cdot 10^{-5} \end{bmatrix} \tag{4.26}$$

The matrices with the operating point inserted becomes

$$A = \begin{bmatrix} 0 & 100 & 0 \\ -57.3580 & -500 & 122.72 \\ 0 & -237.70 & 0 \end{bmatrix} \tag{4.27}$$

$$B = \begin{bmatrix} 0 \\ 0 \\ 3503.8 \end{bmatrix} \tag{4.28}$$

The linearized system is controllable and observable. The transfer function is given by

$$\frac{x_1}{u} = \frac{4.3 \cdot 10^7}{s^3 + 500s^2 + 34906s} \tag{4.29}$$

The eigenvalues of the open loop system are calculated to be

$$p = \begin{bmatrix} -416.11 \\ -83.89 \\ 0 \end{bmatrix}$$

which shows that it is marginally stable. The control input will only be updated every 10th time step, every 10 ms, therefore a time delay of 5 ms which is the average delay, is added to the

open loop transfer function. For calculations, a 2nd order Padé approximation is constructed, using the Matlab function `pade`.

Figure 4.2 shows the open loop bode diagram for the linearized system with the time delay included. It can be seen that the system is stable.

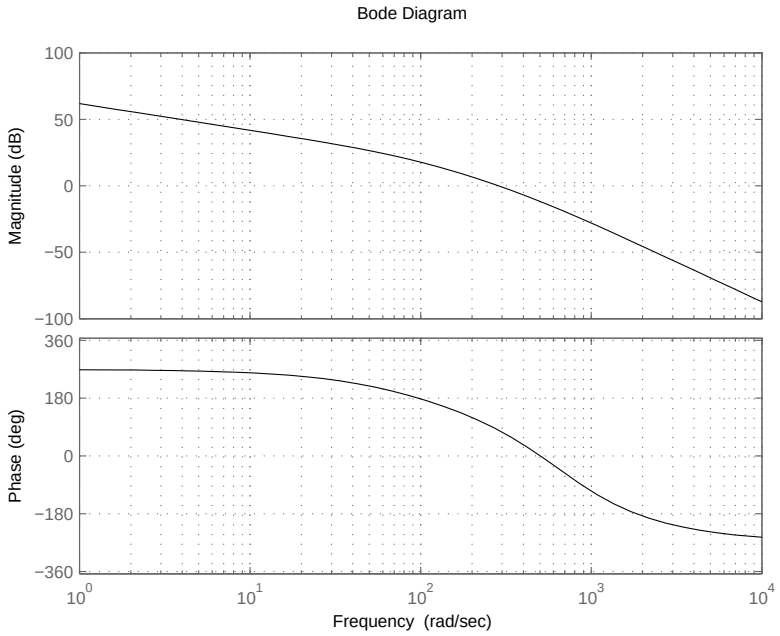

Figure 4.2: Bode diagram for the open loop linearized system.

4.6.3 Control design and tuning

In order to have a proper, i.e. implementable, control system, a proportional controller with limited derivative action[6] will be designed. It will henceforth be called PD controller.

The PD controller will be designed using the Bode-Nyquist criterion, explained in [1]. It is desirable to have a phase margin of 45° at 0 dB, a gain margin of 6dB at 180°, and a not too high bandwidth to reduce the influence of measurement noise. This is a common design goal for linear controllers [1].

The transfer function of the controller is given by [1]

$$h(s) = K_p \frac{1 + T_d s}{1 + \alpha T_d s} \tag{4.30}$$

where $K_p, T_d > 0$ and $\alpha < 1$ is a parameter that limits the derivative action which lowers the phase lag and gain of the overall system at high frequencies.

[6] Often called lead-network.

The controller is going to be implemented in Matlab Simulink, and it is favorable that transfer functions are avoided. Therefore a state space realization of the controller has to be made. By following the algorithm in [2], the following realization is obtained

$$\dot{x} = -\frac{1}{\alpha T_d}x + u \tag{4.31}$$

$$y = \frac{K_p}{\alpha T_d}\left(1 - \frac{1}{\alpha}\right) \tag{4.32}$$

where u is the input to the controller, i.e. the tracking error, and y is the output of the controller, i.e. the input to the plant. The derivation of the realization is analogous to the linear filter in Section 3.1 and is given in Appendix B.1 and is therefore not given in detail.

Tuning based on bode diagram is performed and reasonable values for the controller is found. They are given by

$$K_p = 5.1 \cdot 10^{-2}$$
$$T_d = 2.4 \cdot 10^{-2}$$
$$\alpha = 0.05$$

and yield a gain margin of 6.09 dB at 209 rad/s and phase margin of about 57.4° at 102 rad/s. Bode diagram, with gain and phase margins of the controller in series with the system is given in Figure 4.3.

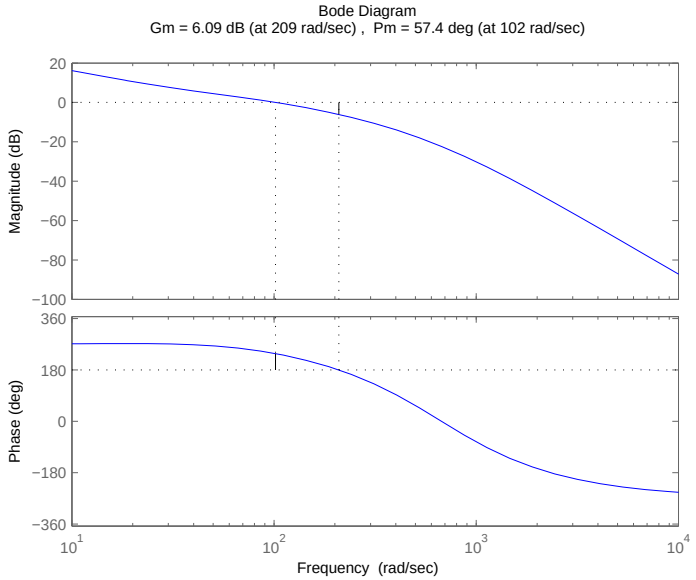

Figure 4.3: Bode diagram for the open loop transfer function of the controller in series with the clutch model.

Simulation under nominal conditions yields the results presented in Figure 4.4. The controller manages to track the reference, but the response of the control system is slow and has a small stationary error, which probably arises from the dead zone of the valves. This effect could

maybe be removed by a controller with integral action. System trajectories seem to overshoot for high position values. The control input is seen to be smooth. Fully clutch engagement is ensured by the controller disengage block when the position approaches zero.

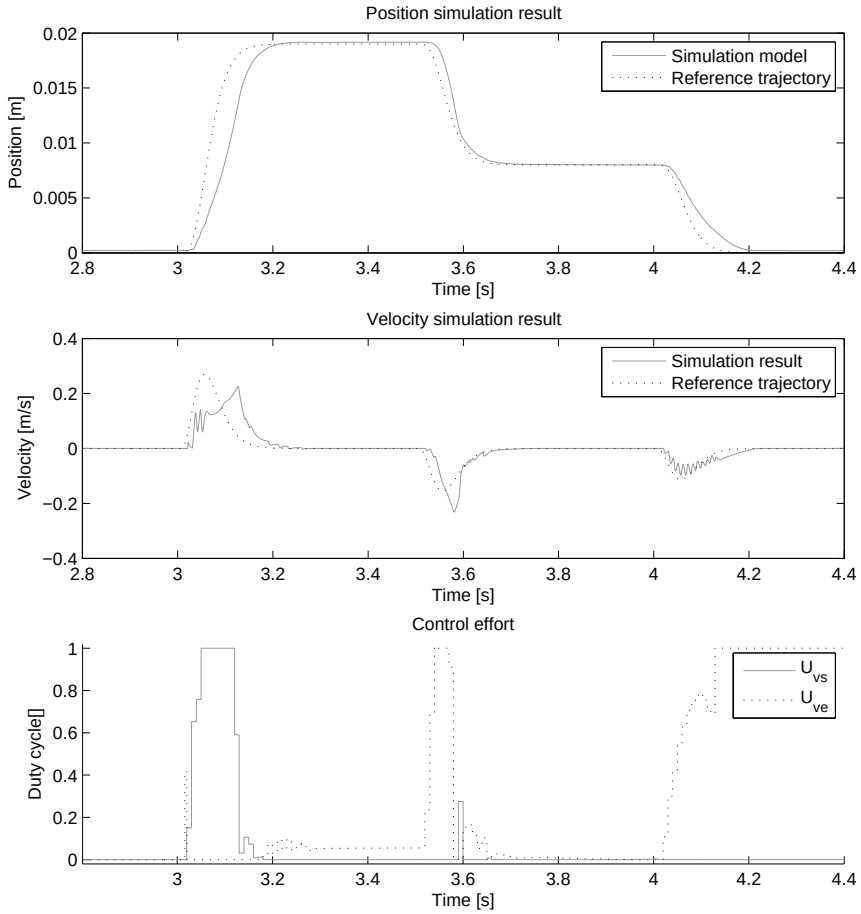

Figure 4.4: Control input and corresponding position and velocity trajectories. PD controller, ODE1, step size 0.001 s.

4.7 Sliding mode controller

In this section the sliding mode controllers of Gjone [4] will be presented together with a modified sliding mode controller that have not yet been applied to the clutch actuator system at Kongsberg Automotive.

Sliding mode controllers suffer from chattering[7] [7], [17], but this effect can be avoided by replacing the signum function by a high-slope saturation function[8], boundary layer control. Another technique is to artificial increase the relative degree of the system by treating the derivative of the real input as the control input [11]. The magnitude of the chattering motion can be decreased by adding the equivalent control to the control law, which cancels known terms of the system dynamics and thus leads to reduction of the magnitude of the switching component.

4.7.1 Normal form

The system (4.1) - (4.3), can be written as a generic system

$$\dot{\boldsymbol{x}} = f(\boldsymbol{x}) + g(\boldsymbol{x})u \tag{4.33}$$
$$y = h(\boldsymbol{x}) \tag{4.34}$$

It has to be written in normal form[9] [7], Section 13.2, for sliding mode control

$$\dot{\boldsymbol{\eta}} = \boldsymbol{f_0}(\boldsymbol{\eta}) \tag{4.35}$$
$$\dot{\boldsymbol{\xi}} = A_c\boldsymbol{\xi} + B_c\gamma(\boldsymbol{x})[u - \alpha(\boldsymbol{x})] \tag{4.36}$$
$$y = C_c\boldsymbol{\xi} \tag{4.37}$$

where (4.35) disappears, because the relative degree equals the order of the system $\rho = n = 3$, and

$$A_c = \begin{bmatrix} 0 & & & \\ 0 & & & \\ \vdots & & I_{\rho-1} & \\ & & & \\ 0 & 0 & \dots & 0 \end{bmatrix}, \; B_c = \begin{bmatrix} 0 \\ \vdots \\ 0 \\ 1 \end{bmatrix}, \; C_c = \begin{bmatrix} 1 & \dots & 0 & 0 \end{bmatrix} \tag{4.38}$$

where the dimension of the matrices are given by the number of the relative degree ρ of the system. The remaining functions of the normal form are given by

$$\gamma(\boldsymbol{x}) = L_g L_f^{\rho-1} h(\boldsymbol{x})$$
$$\alpha(\boldsymbol{x}) = -\frac{L_f^{\rho} h(\boldsymbol{x})}{L_g L_f^{(\rho-1)} h(\boldsymbol{x})}$$

[7] The controller is unable to keep the system on the sliding manifold due to imperfections and delays in the actuator and controller structure. The system will follow a trajectory which oscillates around the sliding manifold. This is called chattering, and will degrade the system accuracy, increase the energy consumption, as well as reduce the lifetime of the system. It may even in some cases be dangerous.

[8] With a high-slope saturation function the sliding mode controller becomes a continuous control law.

[9] The system is written in normal form when the system is described as a chain of integrators and the nonlinearities are only present in the same state as the control input.

where $y = h(\boldsymbol{x})$ is the output of the original system and L is the Lie differentiation operator. For a system with order identical to the relative degree $\rho = n$, a diffeomorphism is given by [7]

$$T(\boldsymbol{x}) = \begin{bmatrix} h(\boldsymbol{x}) \\ L_f h(\boldsymbol{x}) \\ L_f^2 h(\boldsymbol{x}) \end{bmatrix} \tag{4.39}$$

which is the measurement an its time derivatives up to the order of the system. The calculation of the expressions in of the normal form are performed in Section B.2.

The resulting equations are

$$\boldsymbol{\xi} = \begin{bmatrix} y \\ v \\ \frac{1}{M}(Ap - Ap_0 - f_l(y) - D_v v) \end{bmatrix} \tag{4.40}$$

$$\begin{aligned} \dot{\boldsymbol{\xi}}_3 = \frac{1}{M}\left(-\frac{\partial f_l(\xi_1)}{\partial \xi_1}\xi_2 - \frac{D_v}{M}\xi_3 - \frac{A}{V(\xi_1)}\xi_2(M\xi_3 + Ap_0 + f_l(\xi_1) + D_v\xi_2)\right) \\ + \frac{ART_0}{MV(\xi_1)}u \end{aligned} \tag{4.41}$$

4.7.2 Ideal sliding mode controller

The purpose of sliding mode controllers is to control the system to a state where the scalar value σ to zero, where σ defines a surface of system variables. The sliding surface is given by

$$\sigma = a_1 e_1 + a_2 e_2 + e_3 \tag{4.42}$$

which ensures that the control input u is not present in σ, because the relative degree of the system $\rho = 3$, but in its first derivative

$$\begin{aligned} \dot{\sigma} &= a_1\dot{e}_1 + a_2\dot{e}_2 + \dot{e}_3 \\ &= a_1 e_2 + a_2 e_3 + \dot{e}_3 \\ &= f(\boldsymbol{\xi}) + g(\boldsymbol{\xi})u - y_r^{(3)} + a_1 e_2 + a_2 e_3 \end{aligned} \tag{4.43}$$

where the tracking error is given by

$$e_i = y_r^{(i-1)} - y^{(i-1)} \tag{4.44}$$

for $i \in \{1, 2, 3\}$ and $y_r^{(i-1)}$ is given by the reference trajectory filter in Section 4.2.

The control law is defined as

$$u = u_{eq}(\boldsymbol{\xi}) - \beta(\boldsymbol{\xi})\mathrm{sgn}(\sigma) \tag{4.45}$$

where $u_{eq}(\boldsymbol{\xi})$ is the equivalent control which cancels known terms in (4.42) and $\beta(\boldsymbol{\xi})$ is the gain of the switching component of the control law.

The equivalent control is given by

$$u_{eq} = \frac{1}{g(\boldsymbol{\xi})}[-\hat{f}(\boldsymbol{\xi}) - a_1 e_2 - a_2 e_3 + y_r^{(3)}] \tag{4.46}$$

where $\hat{f}(\boldsymbol{\xi})$ is a approximation of $f(\boldsymbol{\xi})$ and it is assumed that

$$|f(\boldsymbol{\xi}) - \hat{f}(\boldsymbol{\xi})| \leq C_F \tag{4.47}$$

A Lyapunov-like[10] function candidate is

$$V(\sigma) = \frac{1}{2}\sigma^2 \tag{4.48}$$

and differentiation yields

$$\begin{aligned}
\dot{V}(\sigma) &= \sigma\dot{\sigma} \\
&= \sigma\left(f(\boldsymbol{\xi}) - y_r^{(3)} + a_1 e_2 + a_2 e_3 + g\left(\boldsymbol{\xi}\right)(u_{eq} - \beta(\boldsymbol{\xi})\text{sgn}(\sigma))\right) \\
&= \sigma\left(f(\boldsymbol{\xi}) - \hat{f}(\boldsymbol{\xi})\right) - g(\boldsymbol{\xi})\beta(\boldsymbol{\xi})|\sigma| \\
&\leq |\sigma|C_F - \left(g(\boldsymbol{\xi})\beta(\boldsymbol{\xi})\right)|\sigma| \\
&\leq -(g(\boldsymbol{\xi})\beta(\boldsymbol{\xi}) - C_F)|\sigma|
\end{aligned} \tag{4.49}$$

which can be made negative semidefinite

$$\dot{V} \leq -G_0 k_0 |\sigma| \tag{4.50}$$

by choosing $\beta(\boldsymbol{\xi}) = \frac{C_F}{G_0} + k_0$, $k_0 > 0$ and $0 < G_0 \leq g(\boldsymbol{\xi})$. The origin of the system can be shown to be global asymptotic stable [4]. By comparing (B.18) and (B.19) it is found that

$$g(\boldsymbol{\xi}) = \frac{ART_0}{MV(y)} \tag{4.51}$$

The least upper bound of $g(\boldsymbol{\xi})$ is found by taken the largest volume $V(y)$ possible, given by

$$\begin{aligned}
V_{max}(y) &= V_0 + Ay_{max} \\
&\approx 5.162 \cdot 10^{-4}\ \text{m}^3
\end{aligned} \tag{4.52}$$

when $y_{max} = 0.03$ m. Inserting $V_{max}(y)$ and the constant values yields

$$G_0 = 1.997 \cdot 10^5\ \text{J/kg}^2\text{m}^2 \tag{4.53}$$

The constant C_F can be obtained in the following way. The estimation error

$$\tilde{f} = f(\boldsymbol{\xi}) - \hat{f}(\boldsymbol{\xi}) \tag{4.54}$$

is hard to calculate, because the simulation model, which is the best description of the system dynamics available, leads to complex equations for $f(\boldsymbol{\xi})$, and they are only estimates too. Therefore an estimate of $\tilde{f}(\boldsymbol{\xi})$ will be obtained by using spline estimates of the measurements. By rearranging (B.18) it is seen that

$$f(\boldsymbol{\xi}) = \dot{\boldsymbol{\xi}}_3 - g(\boldsymbol{\xi})u \tag{4.55}$$

[10] The suggested function is only Lyapunov-like, because it is not necessary for all states to be equal zero for the function value to be equal zero.

This is inserted in (4.54)

$$\begin{aligned}\tilde{f}(\boldsymbol{\xi}) &= \dot{\boldsymbol{\xi}}_3 - g(\boldsymbol{\xi})u - \hat{f}(\boldsymbol{\xi}) \\ &= y^{(3)} - \frac{ART_0}{MV(y)}u - \hat{f}(\boldsymbol{\xi})\end{aligned} \tag{4.56}$$

To get smooth derivatives of the position measurement, spline estimates is used for y and $y^{(3)}$. By applying the same control input that is used in the measurements, $\hat{f}(\boldsymbol{\xi})$ is obtained. The measurement sample used is taken from an experiment where the clutch tracks a fast varying reference, using another controller, which is expected to enforce the largest error of the friction model. A major problem is that only the control input to the valves are available, and not the flow which is the control u in the control design model (4.3). This method is used because it is considered to get the best possible estimate of $\tilde{f}(\boldsymbol{\xi})$. The estimation error is shown in Figure 4.5 and the maximum absolute error is found to be $1.5924 \cdot 10^4$ N/kgs. Therefore $C_F = 1.593 \cdot 10^4$N/kgs would be a reasonable choice.

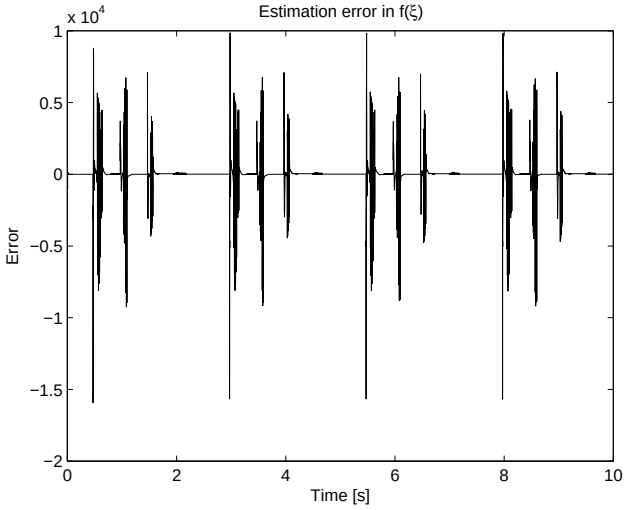

Figure 4.5: Estimation error $\tilde{f}(\boldsymbol{\xi})$.

The rest of the controller constants a_1, a_2 and k_0 are to be determined based on controller testing.

The ideal sliding mode is not usable in practise, because it will induce chattering. Therefore it will not be investigated further in this report. Simulation results for the ideal sliding mode controller with $a_1 = 10^5$, $a_2 = 10^3$ and $k_0 = 0.01$ are shown in Figure 4.6. Complementary plots are shown in Figure C.4 - C.7. Simulation model states are used in the expressions for u_{eq} and σ.

It can be seen that the controller easily saturates the control valves. The controller follows the trajectory satisfactorily, but chattering is observed. The chattering starts when the sliding surface is crossed, around $t = 3.15$ s. The simulation model render low damping, possibly increasing the chattering effect in combination with the PWM control method. Oscillations in the acceleration may degrade the controller performance through the equivalent control directly, or causing high values for a_1 and a_2 to be chosen. The oscillations may arise from

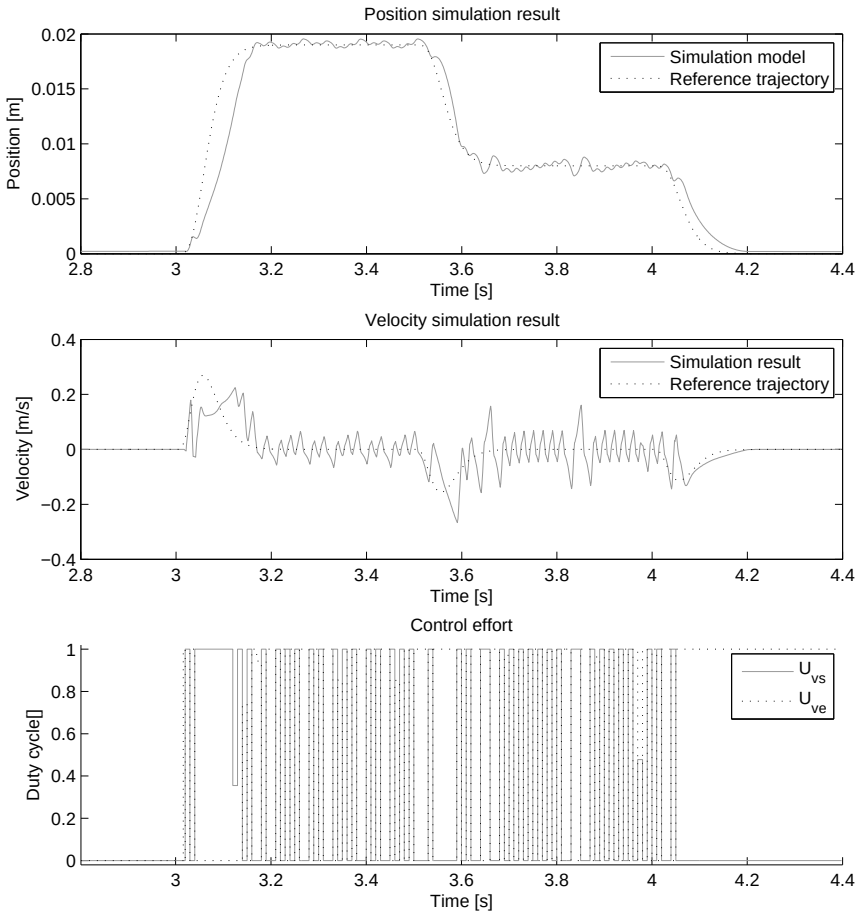

Figure 4.6: Control input and corresponding position and velocity trajectories. Ideal sliding mode controller, ODE1, step size 0.001 s.

the pulse-width modulation together with the low damping of the system. It may be expected that filter use can suppress the oscillations' effect on the controller.

Switching in σ may improve the performance in low speed tracking in case of frictional effects, such as stiction, provided that the switching frequency is well beyond significant vibration modes [16]. This could be exploited in the clutch actuator system. The problem is that the dynamics of this system are so fast that the switching frequency is too low.

4.7.3 Boundary layer controller

One way of avoiding the chattering phenomena is to replace the signum function by a high-slope saturation function in the switching law of the controller, which gives a smooth transition

from -1 to 1 [7]. The controller now becomes continuous[11]. The control law is given by [7]

$$u = u_{eq}(\boldsymbol{\xi}) - \beta(\boldsymbol{\xi})\text{sat}\left(\frac{\sigma}{\epsilon}\right) \tag{4.57}$$

where $\epsilon > 0$ is small number called the boundary layer thickness, which determines the slope of the function. The equivalent control u_{eq} is kept as in (4.46). Therefore the boundary layer controller acts identical to ideal sliding mode controller when $\sigma \geq \epsilon$, which means if the ideal sliding mode is globally asymptotic stable, the boundary layer controller will force the trajectories to enter the set $|\sigma| \leq \epsilon$ [4], but they are not guaranteed stay there, because that depends on the stability inside the boundary layer. To analyse the stability inside the boundary layer, continuous control analyse methods such as linear system design tools can be used [17], and if necessary on a linearized system as in [4]. Even if the system is unstable in the boundary layer, the motion can be no worse than oscillatory, since the switching law outside the boundary layer will force the system to enter the boundary layer. A small ϵ will increase the accuracy in the ideal case, but may introduce chattering when chosen too small [7].

The stability analysis inside the boundary layer will therefore be performed by investigating the poles of a linearization of the feedback system on normal form, for all feasible clutch positions.

The system has to be written in the error dynamics [4]. The error vector is given by

$$e_n = \xi_n - y_r^{(n-1)} \tag{4.58}$$

for $n \in \{1, 2, 3\}$. By expressing the error dynamics in the system equations (4.36), (4.38) and (4.41), the following equilibrium point $\dot{\boldsymbol{e}} = \boldsymbol{0}$, is found

$$\boldsymbol{e}^* = \boldsymbol{0} \tag{4.59}$$

The linearized error system with the controller inserted is a autonomous system. It is given by

$$\boldsymbol{\Delta}\dot{\boldsymbol{e}} = A\boldsymbol{\Delta}\boldsymbol{e} \tag{4.60}$$

where

$$A = \begin{bmatrix} 0 & 1 & 0 \\ 0 & 0 & 1 \\ -\frac{ART_0}{MV(\xi_1)}\frac{\beta}{\epsilon}a_1 & -a_1 - \frac{ART_0}{MV(\xi_1)}\frac{\beta}{\epsilon}a_2 & -a_2 - \frac{ART_0}{MV(\xi_1)}\frac{\beta}{\epsilon} \end{bmatrix} \tag{4.61}$$

which will be stable for a large number of $a_1, a_2 > 0$.

Manual tuning of the boundary layer controller shows that there is a trade off between chattering and controller performance. Proper performance together with smooth control input seem infeasible. Attempts to make the controller produce non-aggressive input, result in chattering with lower frequency, which is shown in Figure 4.7. Therefore the boundary layer controller will not be further investigated in this report. A modification of the boundary layer method which deals with this problem is presented in the next section.

[11] A PD-controller with a very high gain will act quite similar to a boundary layer controller in the presence of saturation limits in the actuators, which are in practise always present.

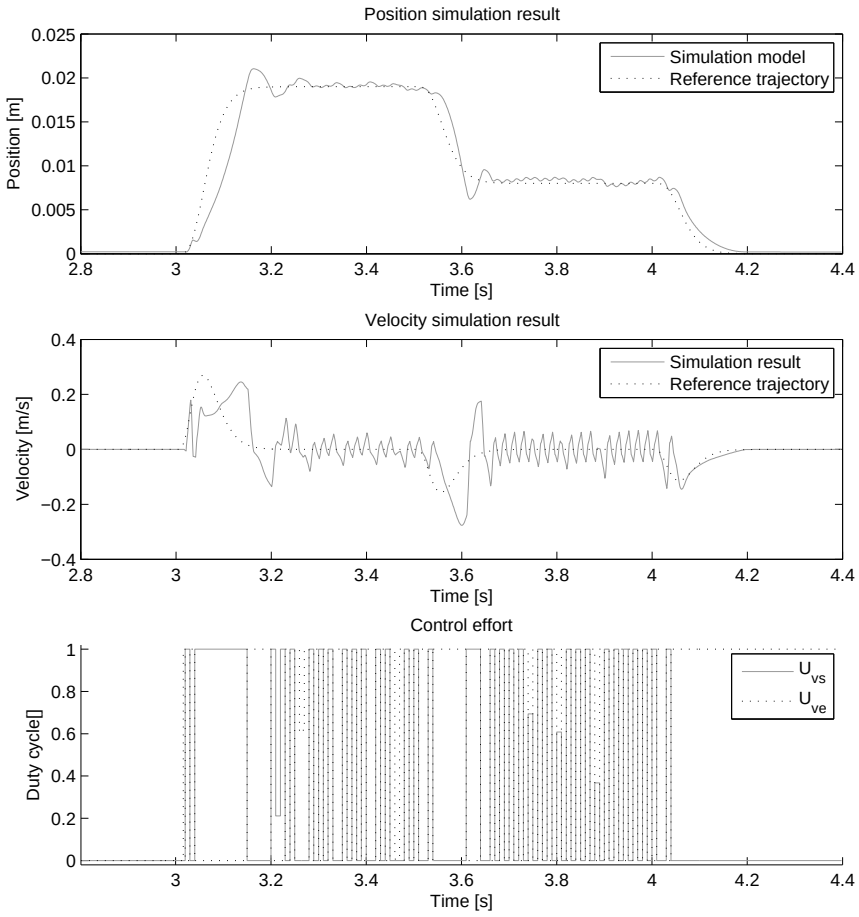

Figure 4.7: Control input and corresponding position and velocity trajectories. Boundary layer sliding mode controller, ODE1, step size 0.001 s, $a1 = 10^4$, $a2 = 1$, $\epsilon = 1$.

4.7.4 Variable boundary layer sliding mode controller

To utilize available bandwidth, the boundary layer width may be adjusted online [16]. In this report the boundary layer will be made time variable for the purpose of obtain sufficient bandwidth for tracking reference trajectories, and intentionally release bandwidth when the position reference is constant[12]. Further the equivalent control term u_{eq} of the boundary layer controller (4.57) will be removed to make it more robust against modeling errors and measurement noise. The controller is given by

$$u = -\beta \text{sat}(\sigma(\alpha|\dot{y}_r| + k)) \tag{4.62}$$

where k is a small number which is included to avoid a gain of zero and α is a tuning parameter that determines the aggressiveness of the controller during transients in the reference. A larger

[12] The lowered bandwidth may introduce risk of poor control in case of disturbances.

k will make the behavior of the controller more like a ideal sliding mode controller, and therefore has to be set small.

Stationary error or slow convergence problems can be improved by filtering the reference trajectory $y_r^{(1)}$. For example the filter may let $y_r^{(1)}$ through when its absolute value is increasing, and low pass filter it when the absolute value is decreasing, or simply consist of a rate limiter to ensure that the value is decreasing slowly.

An implementation of a slow fall-off filter is Shown in Figure 4.8. The filter compares the output of a rate limiter block with the absolute value of the input. If the output of the rate limiter block is larger than the input, the integrator is reset and the low pass filtered reference is the output of the filter. A demonstration of the slow fall-off filter is shown in Figure C.3.

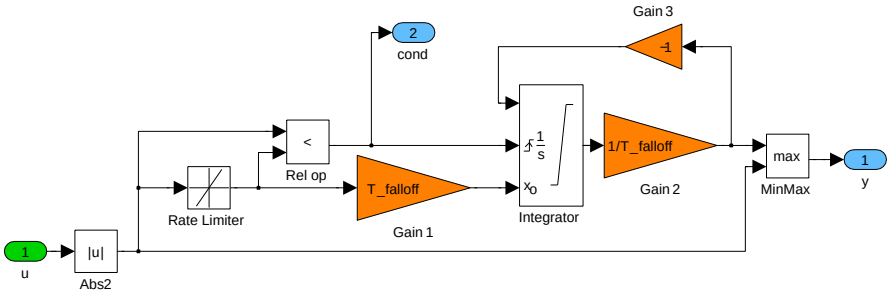

Figure 4.8: Simulink implementation of the slow fall-off filter.

Simulation results are shown in Figure 4.9 and the corresponding sliding surface in Figure 4.10. The controller performs well and chattering is avoided when the reference is constant. One must remember that the dead zone in the valves may degrade the performance when the error is small. A small overshoot similar to the PD controller response is observed at high positions.

4.7.5 2-sliding mode controller

The chattering phenomena can be eliminated by artificially increasing the relative degree of the system by treating the derivative of the real input as the control input and let a 2-sliding mode controller[13] [14] calculate the input, and integrate it before it is put into the rest of the control system. Since the switching control input is integrated, it will be smoother than a pure switching input. The downside is that the derivative $\dot{\sigma}$ of the sliding surface has to be calculated, which in this case means that the third derivative of the position measurement is used in the control law, introducing possible trouble with noisy measurements. This technique also introduces integral action in the controller, which is an advantage.

One 2-sliding mode controller is given by [12]

$$u = -\alpha \frac{\dot{\sigma} + |\sigma|^{1/2} \operatorname{sgn}(\sigma)}{|\dot{\sigma}| + |\sigma|^{1/2}} \tag{4.63}$$

[13] 2-sliding mode occurs when the system trajectories is held at the sliding surface as well as its first derivative, $\sigma = 0$ and $\dot{\sigma} = 0$.

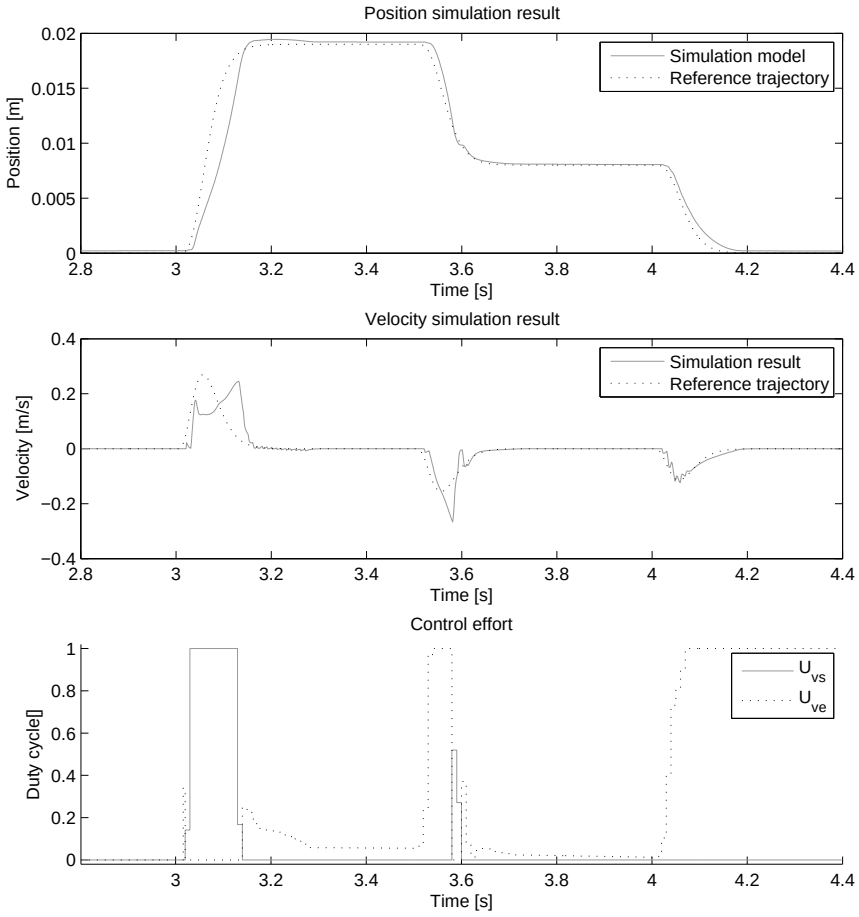

Figure 4.9: Control input and corresponding position and velocity trajectories. Variable boundary layer sliding mode controller, ODE1, step size 0.001 s, $a1 = 10^5$, $a2 = 10^3$, $\alpha = 0.012$, $k = 5 \cdot 10^{-4}$, $T_{falloff} = 1 \cdot 10^{-3}$ s.

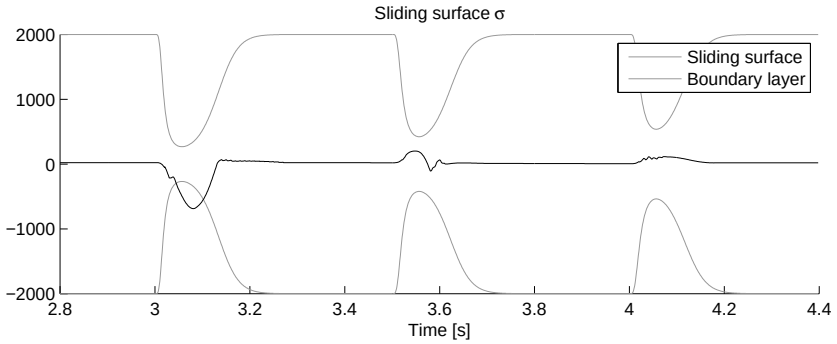

Figure 4.10: Sliding surface and boundary layer width. Variable boundary layer sliding mode controller, ODE1, step size 0.001 s, $a1 = 10^5$, $a2 = 10^3$, $\alpha = 0.012$, $k = 5 \cdot 10^{-4}$, $T_{falloff} = 1 \cdot 10^{-3}$ s.

where α is chosen for any fixed $C, K_m, K_M > 0$ defined by

$$0 < K_m \leq \frac{\partial}{\partial u}\sigma^{(r)} \leq K_M, \quad |\sigma^{(r)}|_{u=0} \leq C \tag{4.64}$$

which must hold at least locally[14].

If α is set high enough, the input u will have such a magnitude that it will go from one saturation limit to the other saturation limit within one time step, thus re-introduce chattering.

To avoid integrator wind-up, a reset signal is taken from the controller disengage block in Section 4.5, such that the integrator is reset and held at reset as long as the condition for controller disengagement is true. There is no risk of clutch re-engagement failure if the integrator has been reset, because the controller disengage block will open the exhaust valve for a period long enough to ensure that the clutch will be fully engaged.

The calculation of $\dot{\sigma}$ needs the third derivative of the measured position, which is performed by differentiating the acceleration estimate by processing it through the LP filter differentiator from Section 3.1.

Simulation results with the 2-sliding mode controller are shown in Figure 4.11 and the corresponding sliding surface is shown in Figure 4.12. It can be seen that the controller performs poorly, even after thorough tuning. Stationary errors are observed and the input resembles chattering-like behavior, although the input is integrated, thus have a lower frequency. The sliding surface value is slowly decreasing when the reference is constant. The controller manages to a certain degree to track the velocity reference with some oscillations.

The stationary position is dependent on the value of α, which is in the author's opinion sign that the controller do not function. It seems that the controller tracks the derivative of the sliding surface $\dot{\sigma}$ well, and may be the reason for the above observation.

A better alternative might be to define the sliding surface as the position error, which will make it necessary to apply a fourth order sliding mode controller to avoid switching in the input. A major drawback with higher order sliding modes are the complexity of the controllers, yielding harder analysis.

[14] The article [12] does not say any more on the choice of α, except that obviously $\alpha < 0$ when $\frac{\partial}{\partial u}\sigma^{(r)} < 0$.

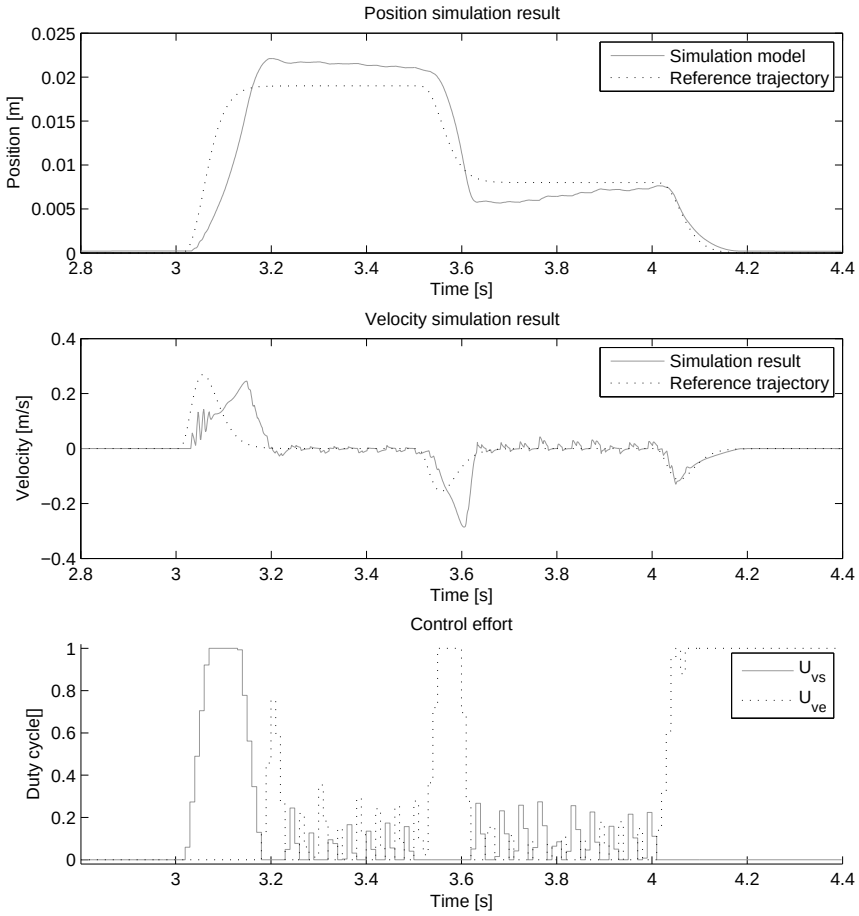

Figure 4.11: Control input and corresponding position and velocity trajectories. 2-sliding mode controller, ODE1, step size 0.001 s, $a1 = 10^5$, $a2 = 10^2$, $\alpha = 0.5$. LP filter time constant $T_{lp} = 10^{-2}$ s.

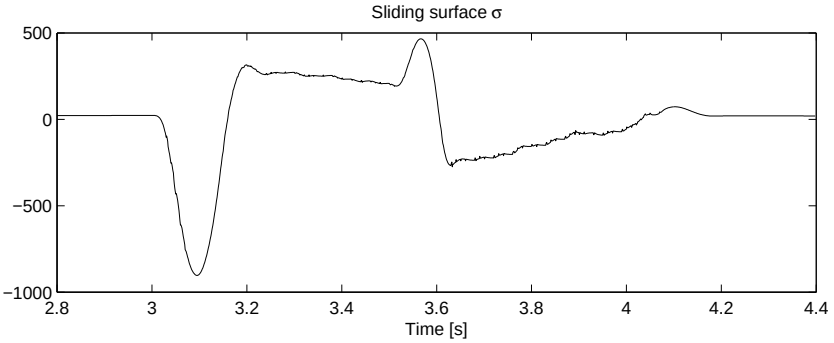

Figure 4.12: Sliding surface. 2-sliding mode controller, ODE1, step size 0.001 s, $a1 = 10^5$, $a2 = 10^2$, $\alpha = 0.5$. LP filter time constant $T_{lp} = 10^{-2}$ s.

Chapter 5

Controller testing

It is important that the clutch controller is both stable and performs well under any circumstances and not only under the assumptions that is made in the design process. The most vulnerable assumptions is considered to be:

1. A specific clutch load $f_l(y)$
2. Constant viscous friction only
3. Constant supply pressure $P_S = 9 \cdot 10^5$ Pa
4. No leakage from the pneumatic system and actuator
5. A certain noise level

The clutch load will alter with age [6]. Friction is dependent on lubrication[1], which is i.a. dependent on the length of the rest period of the actuator. When other pneumatic devices on the truck are in use or in case of pneumatic system failure, the supply pressure may drop and in a critical situation the motor of the truck may stop as a result of clutch disengagement failure. The controller also have to be operative under various environment settings, such as different temperatures, humidity and noise levels.

The measurement filters are robust with reference to parameter variations in clutch and actuator system, since they are, as opposed to observers, only dependent on the system's largest derivatives[2] and measurement noise levels.

It is not feasible to test all combinations of settings or scenarios that may influence the controller performance, therefore a set of parameter test settings is made. The clutch actuator system is nonlinear, which means that the effects of the various test cannot be superpositioned, but it may be assumed that the main tendencies will interact with each other.

Controller robustness comparison will be performed by looking at the root-mean-square error and the maximum absolute error of the clutch position, and investigation of the position, velocity and control input plot as well.

[1] Reported by Kongsberg Automotive.

[2] Under specific conditions, it may happen that the system response is faster than considered in the design process, raising possible problems for slow filters.

5.1 Controller test scenarios

In this section controller robustness test will be performed by application of the PD controller from Section 4.6.3 and the variable boundary layer sliding mode controller (VBLSM) from Section 4.7.4, on the simulation model. Some parameters in the simulation model will be altered while the controllers are kept unchanged, except from a single test.

5.1.1 Clutch load shifting

To simulate a worn clutch, the clutch load characteristic will be shifted 5 mm to the left, see Figure 2.2, i.e. the resting position for the clutch will be -5 mm, and multiplied by 1.10. The hardstop force has to be altered correspondingly, to simulate the new clutch plate surface position.

5.1.2 Friction

The actuator friction will decrease i.a. when the actuator piston is moved for a while. To test the controller response to low friction, the viscous friction will be set to 2000 Ns/m.

5.1.3 Leakage between actuator chambers

A leakage flow of air from chamber A to chamber B, proportional to the relative pressure between the to chambers, will be used to test the controllers' response to leakage.

5.1.4 Controller susceptibility to measurement noise

Measurement noise will always be present in physical systems. The controllers must perform well under the influence of noise. The noise characteristic may changed during operation, in different environments and in series production caused by the components used may differ from prototype components. Since noise is random, a pre-generated noise signal with properties given in Section 2.4 will be added to the position measurement, and applied to all tests.

A test with increased noise will also be performed. No dead signal or wild-point detection logic is included in the controllers, therefore no tests regarding these issues will be accomplished.

5.1.5 Error in the pressure estimate

A test will be performed where the pressure estimate is fixed at 4 bar, which is seen from Figure 4.1 to be not far away from the pressure estimate during the test sequence.

5.1.6 Summary of test scenarios

The test scenarios are:

1. Nominal values
2. $y = -5$ mm, f_l multiplied by 1.10
3. $D_v = 2000$ Ns/m
4. Constant pressure estimate of actuator chamber $\hat{p} = 4 \cdot 10^5$ Pa
5. Leak flow $w_{leak} = 1 \cdot 10^{-9}$ kg/sPa $\cdot (p_A - p_B)$
6. Measurement noise multiplied by 2

All test are performed with measurement noise and with the linear filter for the VBLSM controller.

In addition a test with nominal values of the VBLSM controller with the robust differentiator will be performed[3].

5.2 Controller tests on simulation model

5.2.1 Test 1: Nominal values

This test should view the impact of measurement noise on the controllers . It is expected that the controller performance will be slightly degraded and the control input will be less smooth compared to the design simulation tests in Chapter 4.

The results from the controller tests with nominal values are shown in Figure 5.1 and 5.2. The measurement noise make the PD controller input be oscillating as well as the system response. The controller manages to track the reference to a certain degree. The VBLSM controller make the system follow the trajectory, but overshoots. A small oscillation is seen around the slip point, which may arise from the phase lag that the low pass filter introduces and could probably be reduced by the use of a higher order filter.

The response of both controllers is slow, which most likely stems from the long update intervals of the input. The control input from the VBLSM controller is smoother and does not oscillate around zero, like the intention of the VBLSM is, as it does for the PD controller.

[3]The PD controller is independent of filters and obviously not of interest to be tested with the robust differentiator.

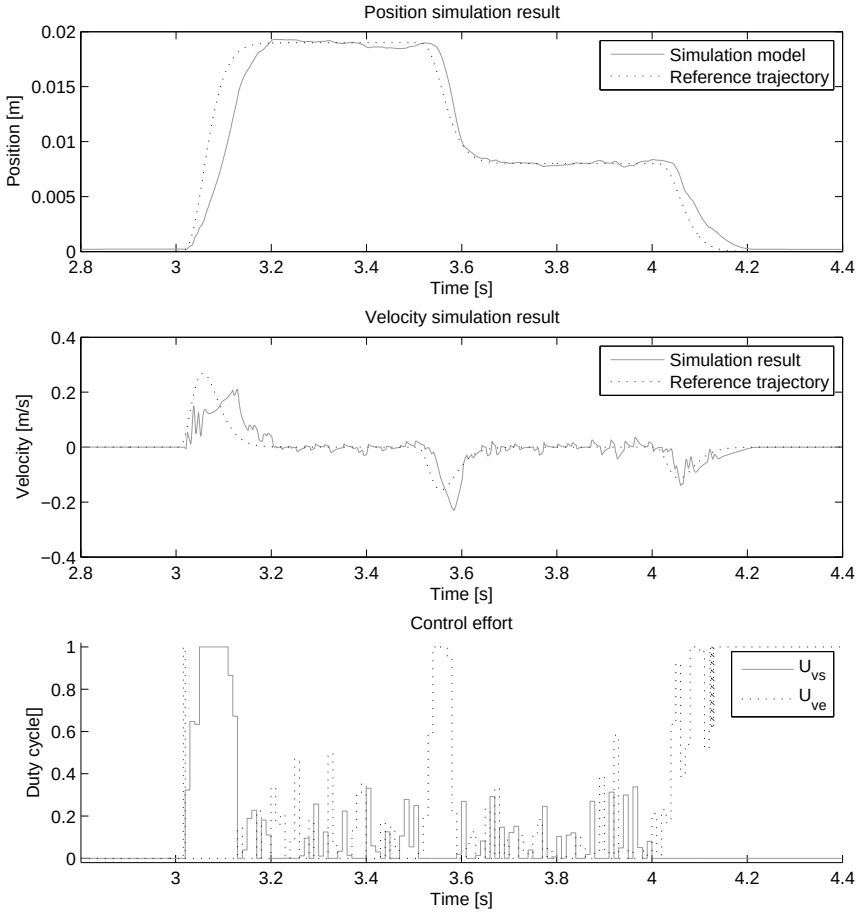

Figure 5.1: Test 1. PD controller

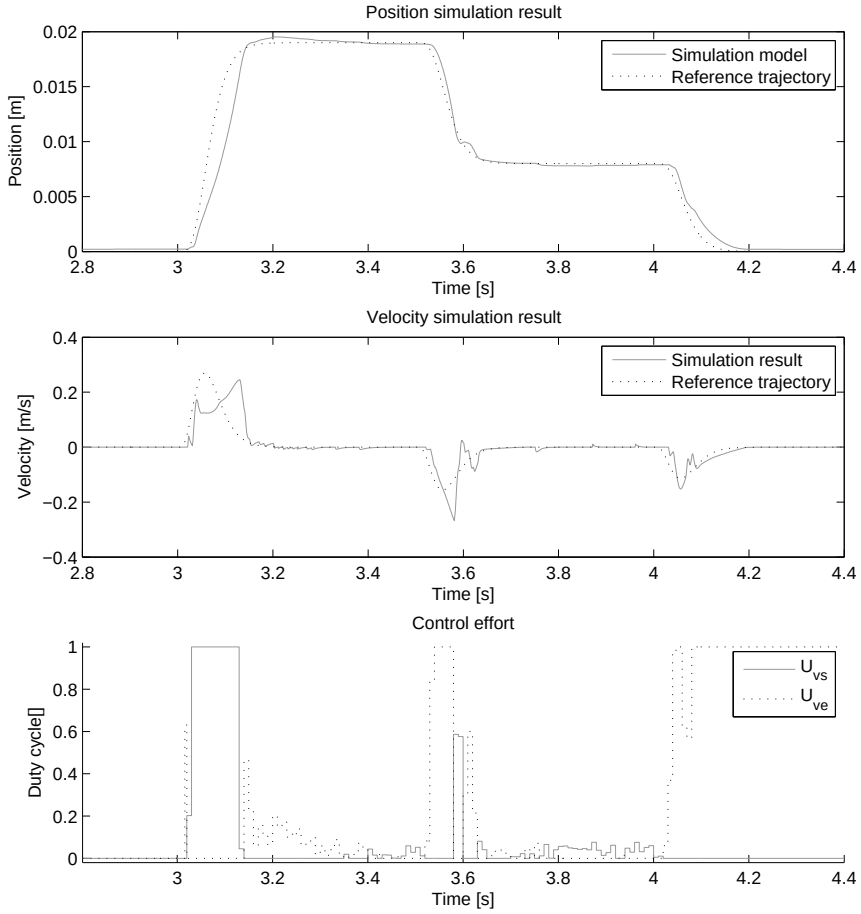

Figure 5.2: Test 1. VBLSM controller

5.2.2 Test 2: Altered clutch spring force

It is expected that increased spring force will yield slower response when the clutch plates are going to be separated and probably contribute to oscillations because the pressure estimate will be wrong, leading to trouble when translating desired flow into valve opening times.

The results from the controller tests with altered clutch spring force properties are shown in Figure 5.3 and 5.4. The PD controller performance is reduced compared to the nominal values test, although the control input is higher as a result of the increased spring force, which may be the reason that the response have oscillations with larger magnitude.

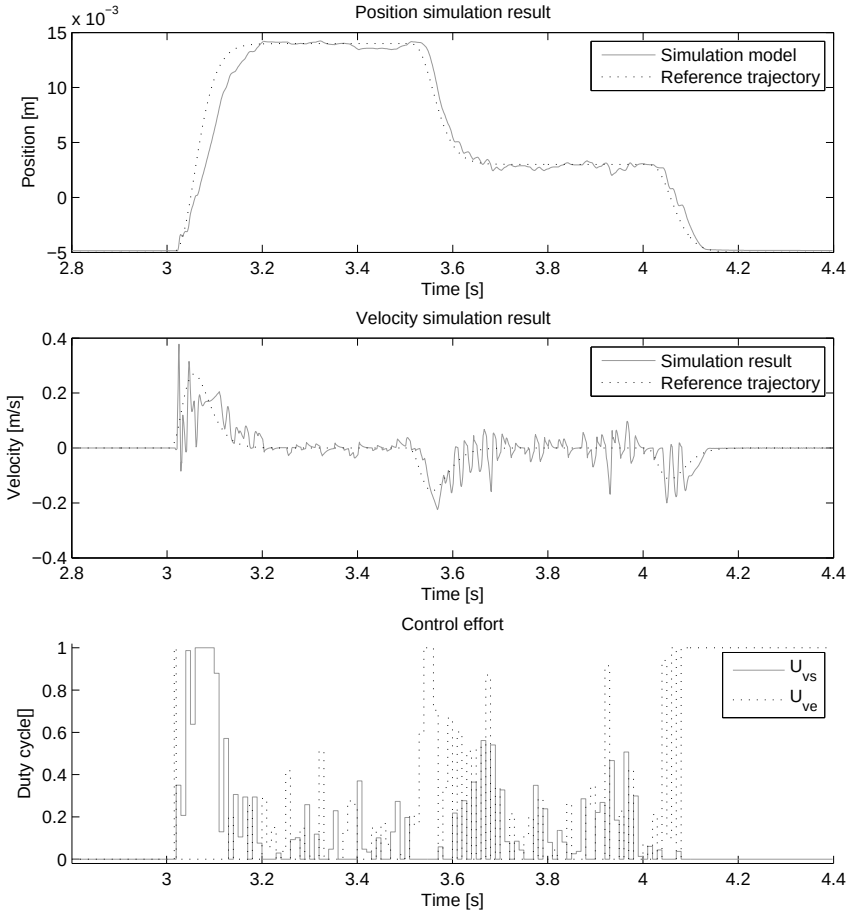

Figure 5.3: Test 2. PD controller

The VBLSM controller output is quite similar and smooth as in the nominal values test. Oscillations around the clutch slip point is observed, which will lead to uneven torque transfer. This may indicate a weakness of the VBLSM controller, that the performance quality drops in transients where the boundary layer is narrower and accurate control is most important.

Notice the good tracking for the VBLSM controller around $4 - 4.1$ s. The response of the

system is quicker, because the spring exerts a stronger force for the corresponding position.

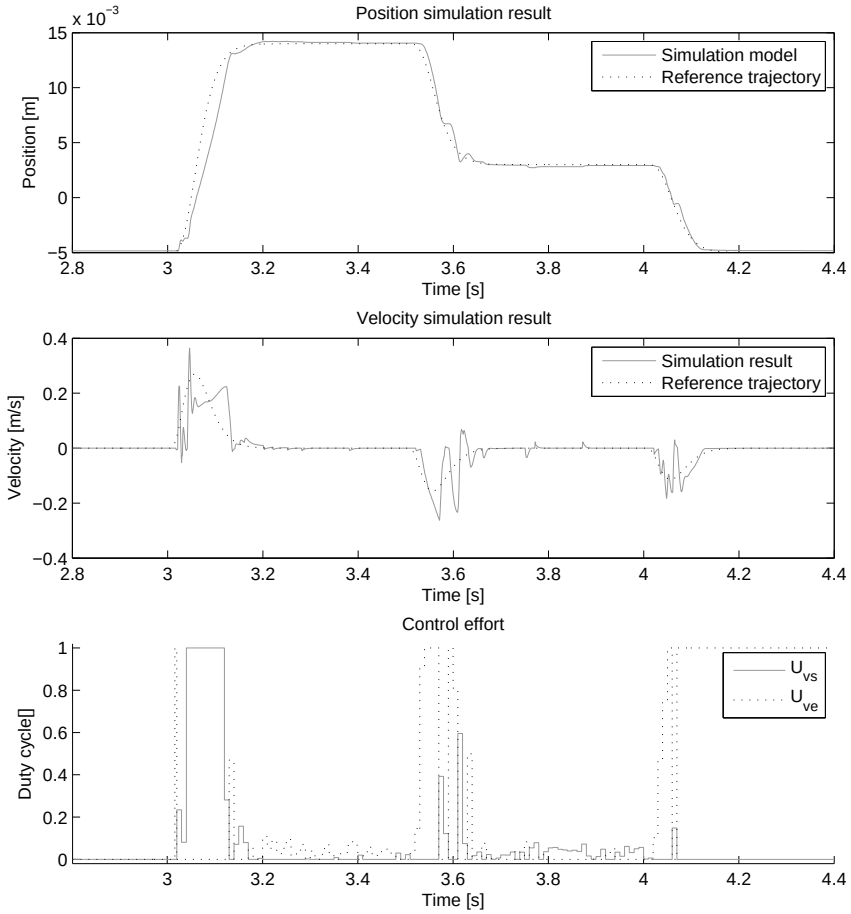

Figure 5.4: Test 2. VBLSM controller

5.2.3 Test 3: Lowered viscous friction

Lowered viscous friction leads to expectations of quicker response and stopping of the actuator piston.

Figure 5.5 and 5.6 show the results from the controller tests with viscous friction $D_v = 2000$ Ns/m. Both controllers seem unaffected by the lower viscous friction which may arise from the fact that the velocity of the clutch is quite low.

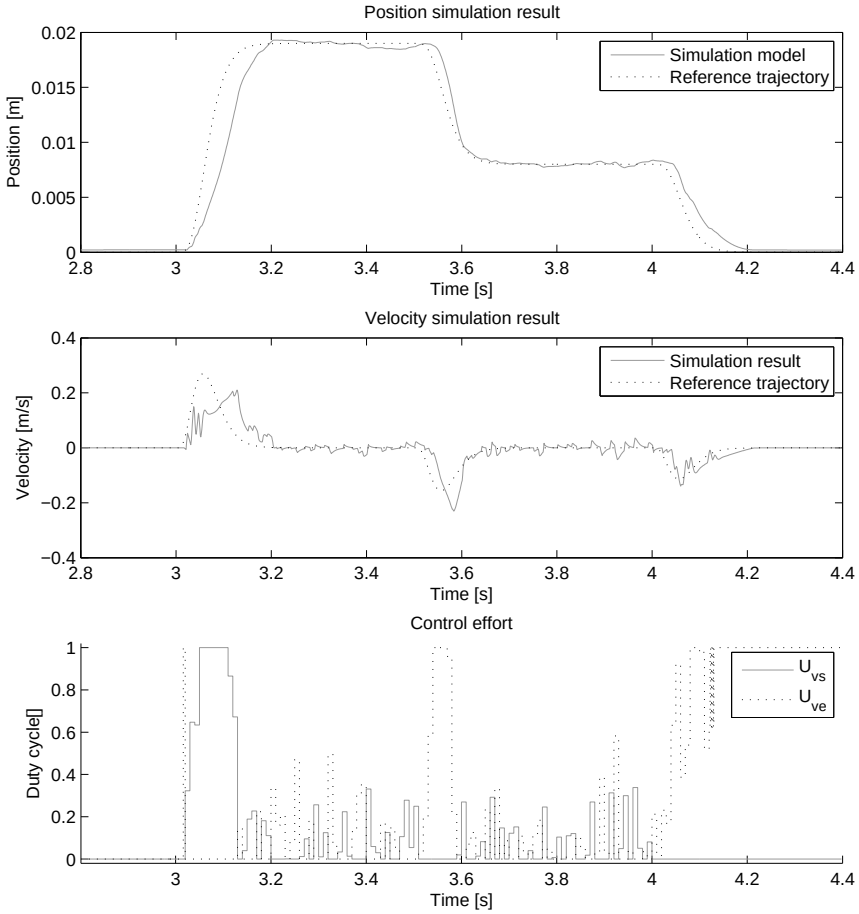

Figure 5.5: Test 3. PD controller

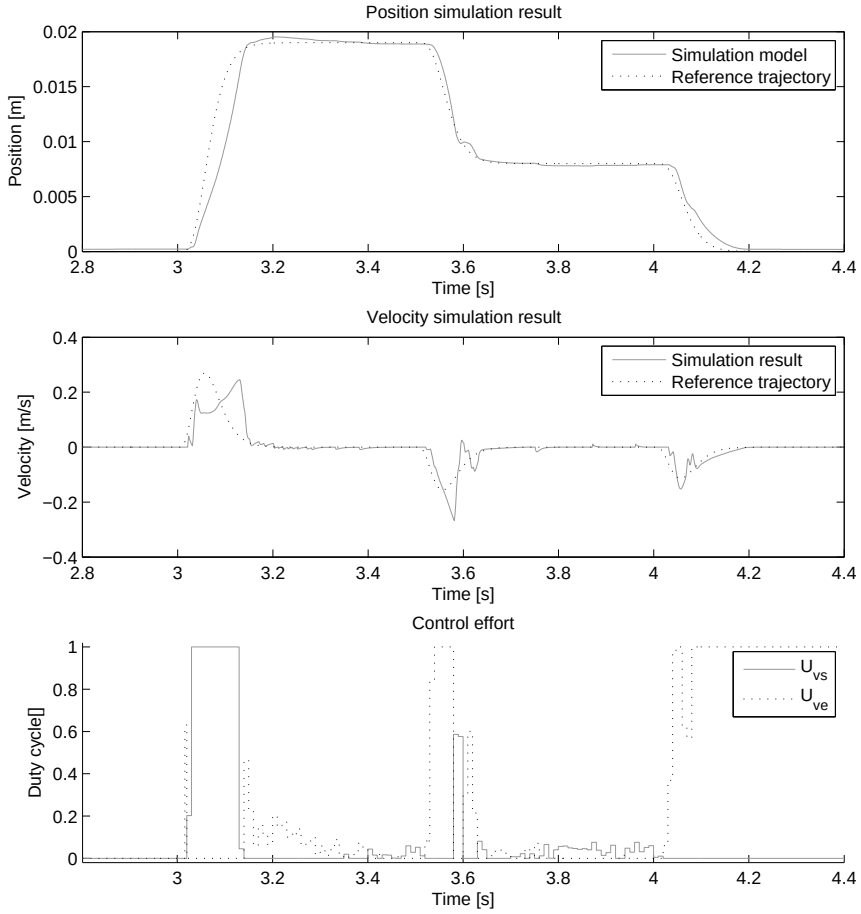

Figure 5.6: Test 3. VBLSM controller

5.2.4 Test 4: Constant pressure estimate

The constant pressure estimate of 4 bar should lead to little difference for a large operating area. For lower positions the high pressure estimate will result in a too high flow expectation, which will make the duty cycle input too low for the supply valve, and vice versa for the exhaust valve. Slower response will be a natural consequence.

The test results shown in Figure 5.7 and 5.8 view hardly noticeable difference from the nominal value test. Then one may ask whether the non-adaptive pressure estimate is necessary. Probably will a slower reference, as will be the case if the reference is taken from the clutch pedal, uncover visible weaknesses with a constant pressure estimate.

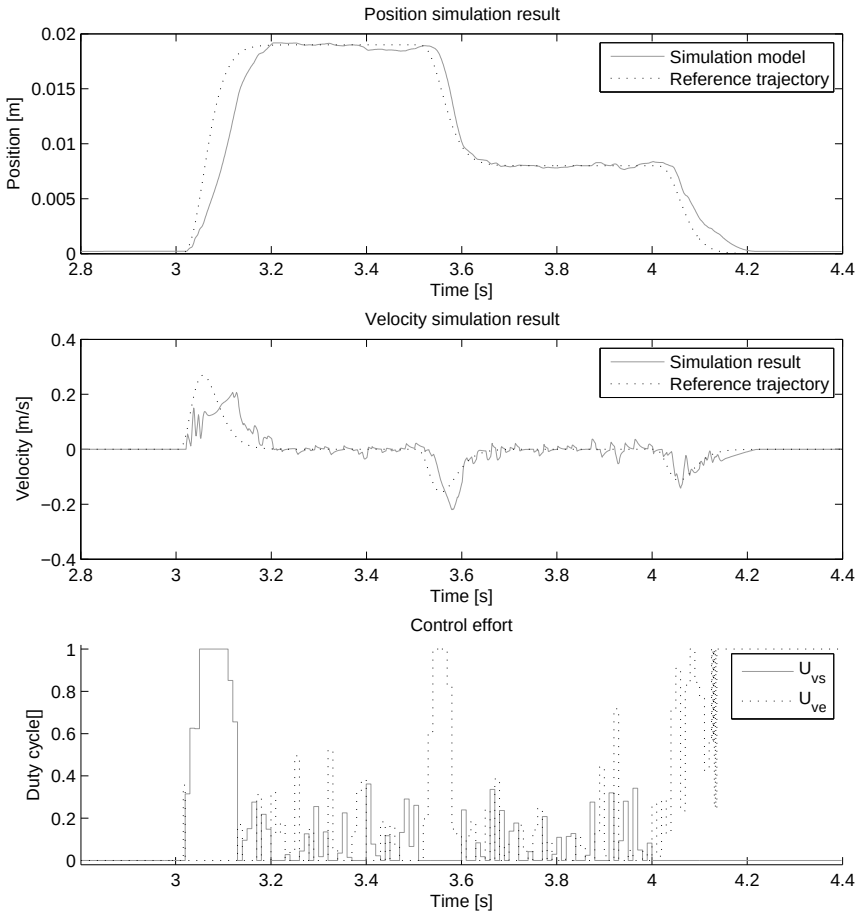

Figure 5.7: Test 4. PD controller

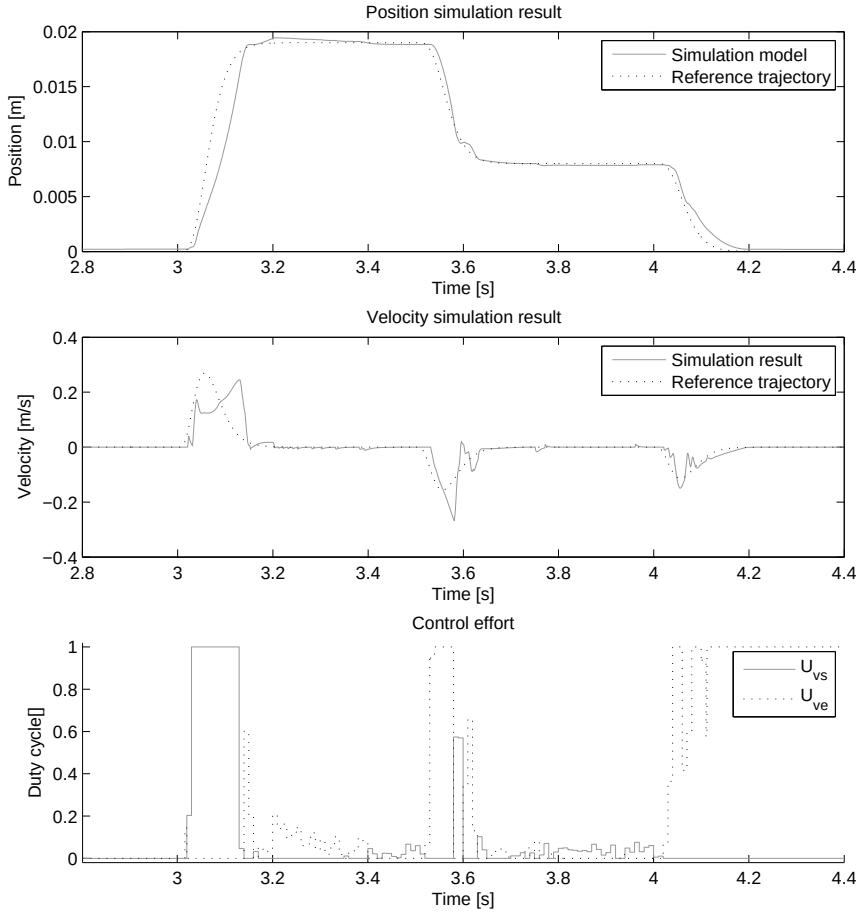

Figure 5.8: Test 4. VBLSM controller

5.2.5 Test 5: Leakage between actuator chambers

Leakage between th actuator chambers will probably lead to slower response under increase in the position reference. Air has to be let into the actuator to compensate for the air that travels to the low pressure side of the piston.

The test plots, Figure 5.9 and 5.10, show that the supply valve has to be used more. Some oscillations is seen for the PD controller, as opposed to the VBLSM controller that handles the leakage well.

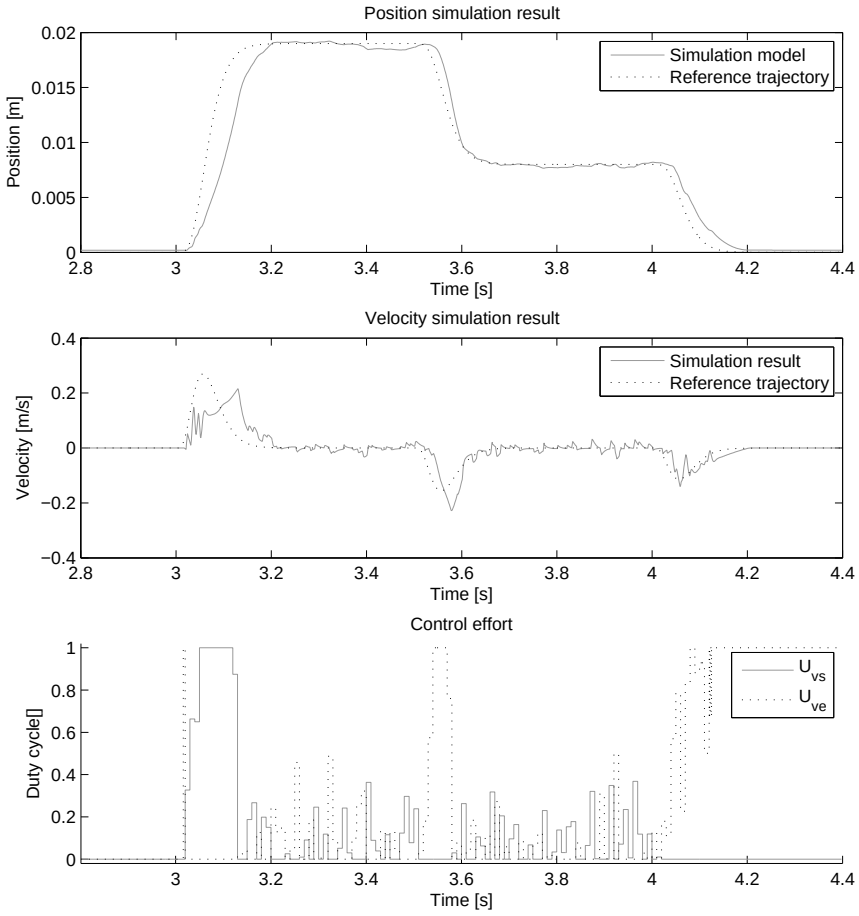

Figure 5.9: Test 5. PD controller

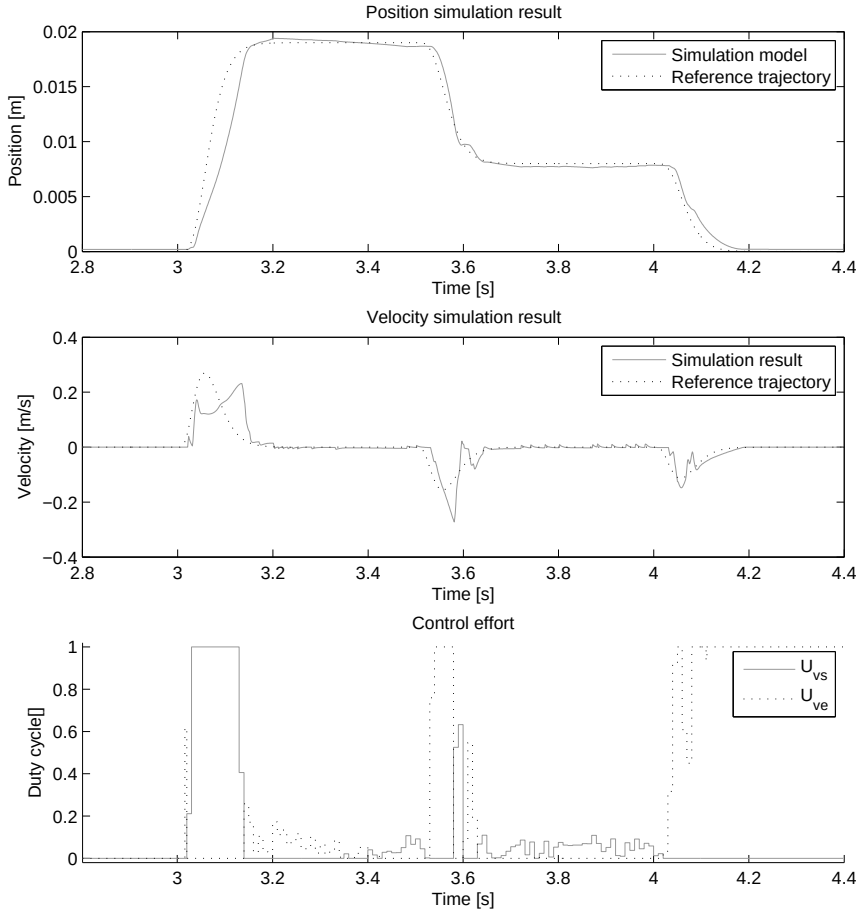

Figure 5.10: Test 5. VBLSM controller

5.2.6 Test 6: Doubled measurement noise magnitude

Increased control effort, oscillatory behavior and decreased accuracy will be a natural expectation of increased measurement noise.

The plots shown in Figure 5.11 and 5.12, indicate that the PD controller is more vulnerable to noise. The VBLSM controller still operates relaxed.

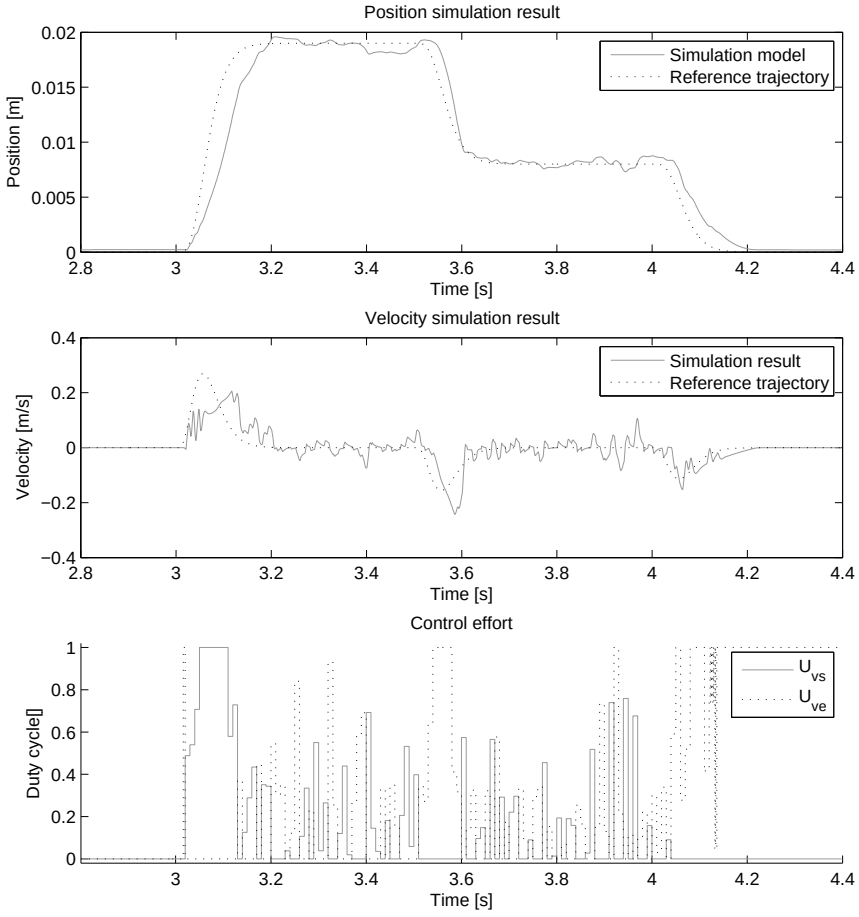

Figure 5.11: Test 6. PD controller

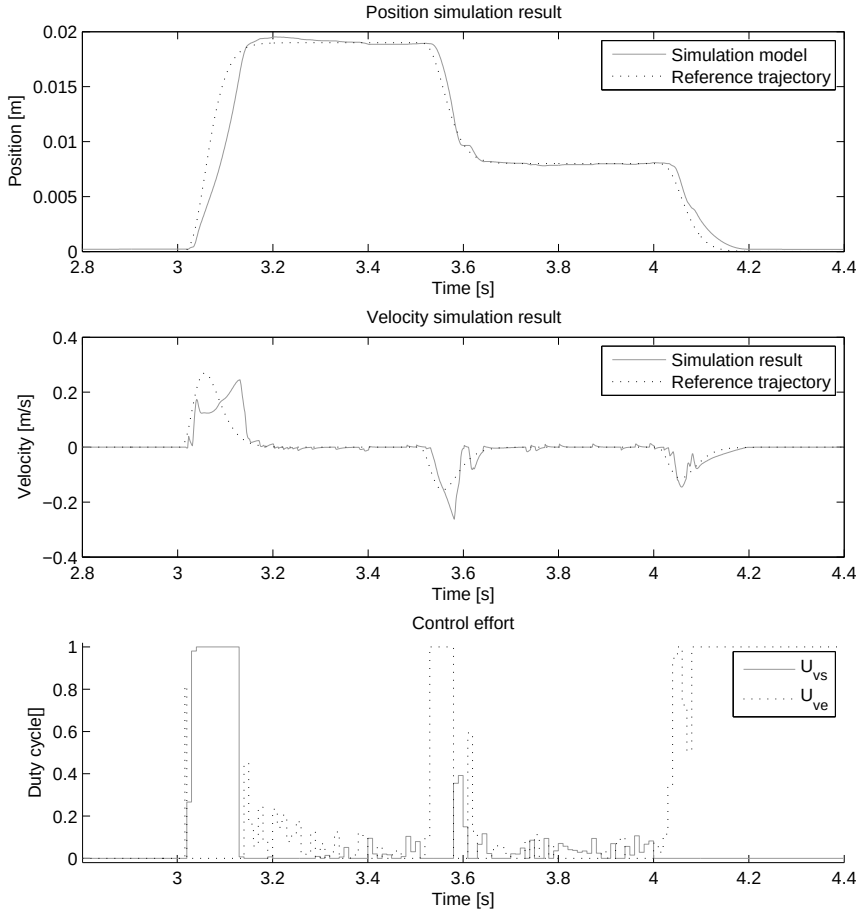

Figure 5.12: Test 6. VBLSM controller

5.2.7 Test of the robust differentiator and VBLSM controller

To test the robust differentiator effect on the controller, a test is run with nominal values. The robust differentiator give oscillatory estimates, which are presented in Section 3.3. It is expected that the result will be similar to Test 6.

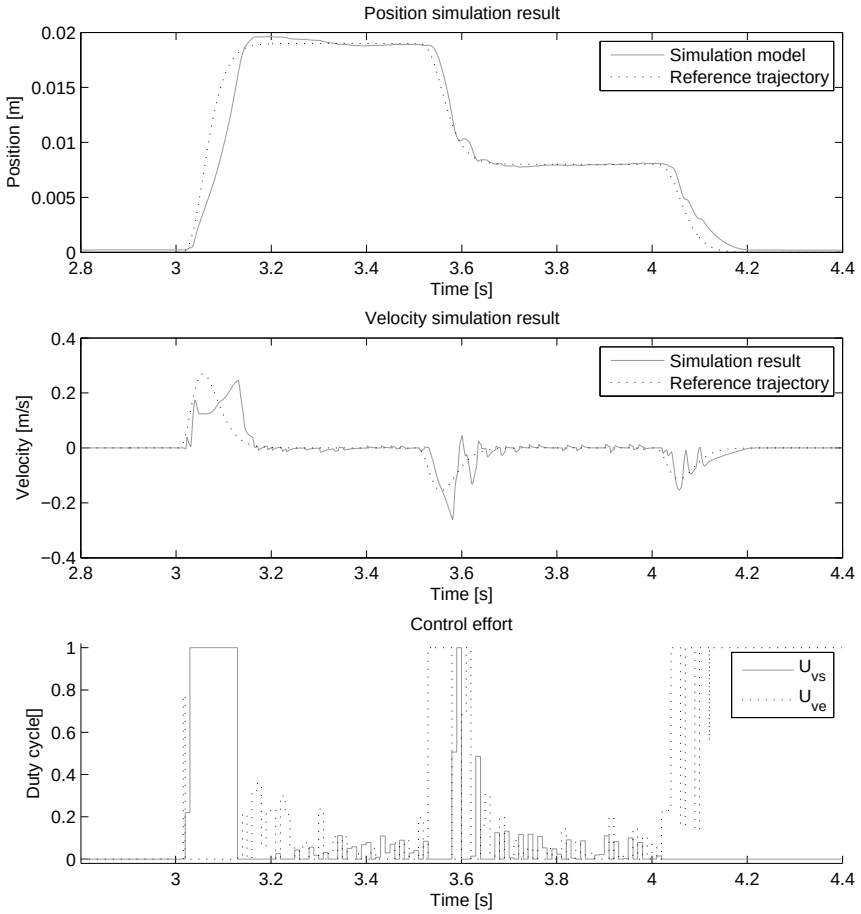

Figure 5.13: VBLSM controller and robust differentiator.

It is difficult to see any significant differences in position between this test and Test 6, but now the control effort is increased, which indicates that a first order low pass filter is a better choice.

5.2.8 Summary of simulation model test results

Test result measures are shown in Figure 5.14. The VBLSM controller performs better in all tests, which may be a result of the tuning procedure. It is tuned to fit this test reference, whereas the PD controller is tuned based on transfer functions and stability analysis.

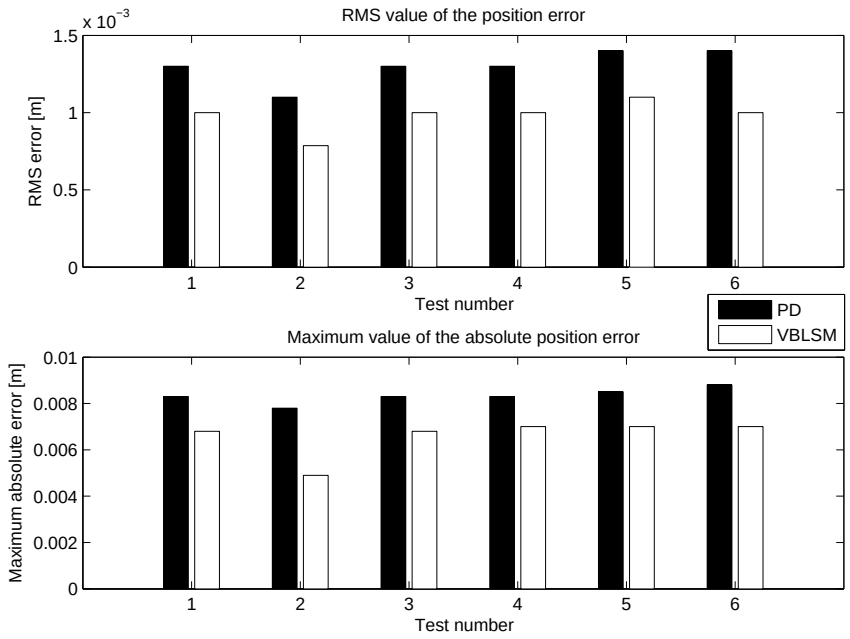

Figure 5.14: Robustness test results of the PD and the VBLSM controller.

The lowest errors are observed in Test 2. It illustrates the importance of the clutch spring in the system, and the clutch force's effect on friction. The VBLSM controller error is significantly lower than for the PD controller, which indicates that it manages to utilize better the extra force exerted by the spring.

Both controllers share the weaknesses on the other tests, which illustrate that they have similar control action. It can be concluded that the robustness of the controllers in these tests are approximately equal, but the performance of the VBLSM controller is better overall.

Test 5 and 6 yields the largest errors, but the differences from the nominal value test are small.

5.2.9 Discussion on the test measure

The test results are compared by looking at the RMS value and the maximum absolute value of the error. It can be argued that other measures would illustrate controller performance better.

It is assumed that the given measures together with visible inspection of the test result plots will give sufficient insight in the controller strengths and weaknesses.

5.3 Controller field test

5.3.1 Test truck

The PD and VBLSM controller were supposed to be tested on a Scania test truck at Kongsberg Automotive. Those controllers were chosen because the VBLSM controller seemed promising and the PD controller where going to be used as a benchmark. The reason that the test were going to performed in a truck and not in a test bench, was that the vibrations from the running engine affects the friction in the clutch actuator. The test truck is shown in Figure 5.15. The clutch spring and actuator arm is shown in Figure 5.16. The control algorithm run on a dSpace MABX 1401 unit. The valves were connected to the actuator chamber via a rubber tubing which in practice extended the volume of the actuator chamber. The increased volume is so small that it will not affect the actuator properties, but the travel time[4] of the air introduces a small time delay.

Figure 5.15: The Scania test truck at Kongsberg Automotive.

The controller implementation in Matlab Simulink is shown in Figure D.5.

Unfortunately, the valve driver circuit, shown in Figure 5.17, went out of order as the tests were about to be performed. The circuit and valves were prototypes had to be used carefully, because they could easily run hot.

No relevant data were saved, but the observations indicated that the controllers caused oscillatory motion. The reason for this was, at that point, the fact that the control input would

[4] The air flow speed in the rubber tubing is constrained by the sonic speed in air.

Figure 5.16: The clutch of the test truck. The clutch spring is seen to the right and the actuator arm is placed vertically to the left.

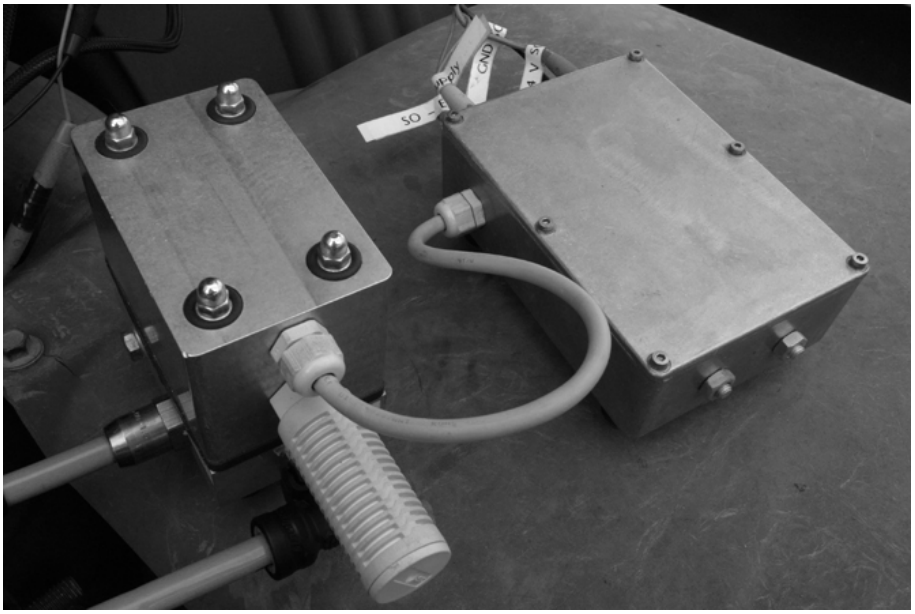

Figure 5.17: The valve driver circuit and valve housing. The air supply tube enters the picture at the left hand side, and the tube that connects the valves to the actuator leaves at the lower left corner. The air from the exhaust valve is released through a muffler.

only be updated at the starting point of the PWM cycle only, and not take the nine[5] previous control inputs into consideration, causing noise to affect the control action as well as the controllers was set up to a too aggressive action since the extra time delay this led to was not considered in the design process. The simulation model and control design then had to be reworked and the new versions are presented in this report.

5.3.2 Planned test scenarios

In this section the test scenarios that were planned to be performed at the test truck are presented.

It is difficult to change the environmental variables under limited test time, therefore most of the tests is performed by altering the pressure estimate in the inverted valve model. The reference used in the control design Chapter 4 were going to be used in the tests.

Test scenarios with changes in pressure estimate:

1. Constant supply pressure of $P_S = 4$ bar
2. Viscous friction $D_v = 2000$ Ns/m
3. Clutch spring force raised 1 kN
4. Clutch spring force lowered 1 kN
5. Nominal values

for both controllers. In addition a test where the reference is taken from the clutch pedal inside the truck were planned.

The maximum absolute error and RMS value of the error were going to be compared for the two controllers.

[5] The PWM cycle is 10 ms and the controller update time step is 1 ms.

Chapter 6

Controller comparison

6.1 PD controller and sliding mode controller comparison

A general PD controller with non-limited derivative action is given by

$$H(s) = K_p(1 + T_d s) \tag{6.1}$$
$$u = K_p(e_1 + T_d e_2) \tag{6.2}$$

The ideal pure switching sliding mode controller, without equivalent control u_{eq}, is given by

$$u = -\beta sgn(\sigma) \tag{6.3}$$
$$\sigma = a_1 e_1 + a_2 e_2 + e_3 \tag{6.4}$$

where e_n is defined as in Section 4.7.2.

The actuator valves has saturation limits on the opening, which leads to variable saturation limits on the air flow, dependent on the pressure inside the actuator chamber. From a performance point of view, β should not be lower than the saturation limit, because this will lead to unnecessarily slow response when the error is large, i.e. a situation where a properly tuned PD controller will saturate the valves.

The PD controller could be extended to include feedback from the acceleration error e_3, which is common in pneumatic actuators [6]. In that case both controllers will be similar, with the only difference that the output of the continuous controller will be depend on the magnitude of the weighted sum of the errors, whereas the switching controller will demand "full throttle", taking only the sign of the weighted sum errors into consideration. Explained trivially, the sliding mode controller is rough.

6.2 Robustness discussion

Stability analysis of a general sliding mode controller under ideal conditions can be found in [7]. The controller (6.3) applied to the clutch system yields the following stability analysis:

A Lyapunov function candidate is given by

$$V = \frac{1}{2}\sigma^2$$

$$\begin{aligned}\dot{V} &= \sigma\dot{\sigma} \\ &= \sigma(a_1e_2 + a_2e_3 + y_r^{(3)} - f(\xi) - g(\xi)\beta\text{sgn}\sigma)\end{aligned}$$

The following assumption is made

$$\left|\frac{a_1e_2 + a_2e_3 + y_r^{(3)} - f(\xi)}{g(\xi)}\right| \leq \varrho(\xi)$$

which yields

$$\dot{V} \leq g(\xi)|\sigma|\varrho(\xi) - g(\xi)\sigma\beta\text{sgn}(\sigma)$$

and choosing

$$\beta(\xi) \geq \varrho(\xi) + \beta_0, \quad \beta_0 > 0$$

ensures that

$$\dot{V} \leq g(\xi)\beta_0|\sigma|$$

Taking $W = \sqrt{2V} = |\sigma|$, which satisfies

$$D^+W \leq g_0\beta_0$$

and by use of the comparison lemma leads to

$$W(\sigma(t)) \leq W(\sigma(0)) - g_0\beta_0 t$$

This means that the system will reach the sliding manifold $\sigma = 0$ in finite time and not leave it. It is obtained without including the equivalent control canceling the known terms, as in (4.45).

It therefore seems fairly easy to ensure that the system is stable under parameter variation, i.e. is robust. The constant or varying gain $\beta(\xi)$ just has to be large enough. The problem is that infinite switching frequency is impossible in practise, which together with limited number precision, inexact system model and more, result in chattering as mentioned in Section 4.7.2.

Another problem with the ideal sliding mode controller is that if the sign of the sliding surface σ is wrong, for example caused by measurement noise, the sliding mode controller will give a large output that is wrong, even if σ has a small value. In that case a PD controller will produce a output with wrong sign too, but the magnitude may be small, leading to more accurate control.

PD controllers are usually tuned using linear analysis, which is dependent on linearization. Lyapunov theory may be used, but in that case it will be difficult to calculate the transient performance of the controller quantitatively. They will of course also suffer from the limited bandwidth of the actuators, with the possibility of oscillatory behavior if not tuned properly, i.e. too aggressive.

The modificated sliding mode controllers, such as the boundary layer controller, will act as a ideal sliding mode controller when the sliding surface is outside the boundary layer. This ensures that the system at least will approach the boundary layer, but only ultimate boundedness related to the boundary layer width ϵ can be proven. For the purpose of avoiding chattering, the boundary layer may have to be set wide, which will lead to difficulties in the investigation of the stability inside the boundary layer as well as removing the favorable robustness properties of the ideal sliding mode controller for a large area of operation and possibly poor control under all circumstances.

Another issue with the boundary sliding mode controllers in this report is that they are tuned by investigation of simulation plots. They are therefore tailored for that reference trajectory, as opposed to the PD controller which is tuned based upon stability measures. It is reasonable to believe that the PD controller may have a better overall performance to different references.

With limited valve opening, a PD controller and a boundary layer controller may be tuned to operate identically, and therefore yield the same robustness properties. The robustness of a boundary layer controller is dependent on tuning in a more compound fashion compared to the ideal sliding mode controller. The controller tests in Section 5.2 show that the PD controller and the VBLSM controller possess approximately the same robustness properties, but as they are tuned, the VBLSM controller performance is higher.

Superfluous use of the valves wears and the lifetime of the actuator system. Therefore a controller that is robust in itself may lead to a less robust system. A robustness improvement can be obtained by introducing redundancy in the valves, such that a single valve error does not lead to total system failure.

It may be concluded that a ideal sliding mode controller is highly robust, but several issues make it not usable in many applications. The modifications applied to the ideal sliding mode controller for the purpose of make it usable also, for the clutch actuator application, remove the properties of that make it robust.

Chapter 7

Conclusion

7.1 Discussion

The ideal sliding mode controller is easy to tune in such a way that the performance is not too bad, but chattering is observed. Chattering is generally unwanted and may have major consequences.

As opposed to literature which may give an impression of that it is relatively easy to avoid chattering by just introducing a boundary layer, the clutch actuator system's stiff dynamics or at least the simulation model's dynamics, make it a hard task to use boundary layer controllers without chattering.

The VBLSM controller performs better than the PD controller under all circumstances. The PD controller tuning is based on gain and phase margins, i.e. mathematical measures of stability and robustness, whereas the VBLSM controller is tuned by investigation of simulation results of the reference trajectory used in the tests. The controller performance degradation under different robustness test is approximately equal. The most significant difference is observed when the clutch spring force is increased. In that case the VBLSM controller yields the lowest tracking error of all tests.

It may be concluded that ideal sliding mode controllers are highly robust, but they are not usable in practise. Modified sliding mode controllers, such as the VBLSM controller yields about the same robustness properties as the PD controller. Adaptive techniques could probably increase the robustness of both controllers.

A variable gain PD controller may have the same benefits as the variable boundary layer sliding mode controller, especially avoiding oscillations when the position reference is constant.

Choices has to be made on controller tuning and it is highly possible that another tuning of both the sliding mode controllers and the PD controller may have yield other results and better performance. The time constant in the reference filter could be adjusted such that the PD controller accuracy became equal to the VBLSM accuracy. The time constants could be compared and it would constitute a measure of the controller quickness.

Tests show that a linear first order filter differentiator for this application achieve at least as

good result as the robust differentiator. The latter has a significantly more intricate structure and is more difficult to tune. The linear filter is straightforward to tune with respect to accuracy and smoothness, and requires less computation.

7.2 Further research

The work carried out to make this report have uncovered different areas that should be investigated further. A more sophisticated measurement filter, perhaps a higher order filter with less phase lag, should be applied to the control system. The filtering technique impact on sliding mode control performance should be also studied more in detail.

The simulation model could be more accurate, especially the valve dynamics model and friction properties, such as the engine vibration's impact on the actuator friction.

All controllers and filters in this report is non-adaptive. Adaptive techniques could make the control algorithms more robust. It is also possible to develop a more robust pressure estimation algorithm, without necessarily construct a full observer.

In-depth analysis of the system dynamics and stability inside the boundary layer could be done. Implementation of sliding mode controllers and their performance in discrete time should be further investigated.

A variable gain PD controller should be compared to boundary layer controllers. The performance of a variable gain PD controller is believed to be comparable with the variable boundary layer controller.

The variable boundary layer controller presented in this report should be tested on the truck, as the intention was.

Bibliography

[1] Jens G. Balchen, Trond Andresen, and Bjarne A. Foss. *Reguleringsteknikk.* Institutt for teknisk kybernetikk, Norwegian University of Science and Technology, 2003.

[2] Chi-Tsong Chen. *Linear System Theory and Design.* Oxford University Press, Inc., 1999.

[3] Olav Egeland and Jan Tommy Gravdahl. *Modeling and Simulation for Automatic Control.* Marine Cybernetics, 2002.

[4] Kristoffer Gjone. Robustness test and analysis of control strategies on an electro-pneumatic actuator. Master's thesis, Norwegian University of Science and Technology, 2007.

[5] Erlend Helgeland. An observer for electro-pneumatic clutch actuation. Project report, Norwegian University of Science and Technology, 2007.

[6] Glenn-Ole Kaasa. *Nonlinear output-feedback control applied to electro-pneumatic clutch actuation in heavy-duty trucks.* PhD thesis, Norwegian University of Science and Technology, 2006.

[7] Hassan K. Khalil. *Nonlinear Systems.* Prentice Hall Inc., 2002.

[8] Kjetil Arne Knudsen. Nonlinear observer design for electropneumatic clutch actuators. Master's thesis, Norwegian University of Science and Technology, 2005.

[9] Hege Langjord, Tor Arne Johansen, Sten Roar Snare, and Christian Bratli. Estimation of electropneumatic clutch actuator load characteristics. In *17th IFAC World Congress, Seoul*, 2008.

[10] Arie Levant. Robust exact differentiation via sliding mode technique. *Automatica*, 34(3), 1998.

[11] Arie Levant. Higher-order sliding modes, differentiation and output-feedback control. *International Journal of Control*, 76(9/10), 2003.

[12] Arie Levant. Quasi-continuous high-order sliding-mode controllers. *IEEE Transactions on Automatic Control*, 50(11), 2005.

[13] Arie Levant. Exact differentiation of signals with unbounded higher derivatives. In *45th IEEE Conference on Decision and Control*, 2006.

[14] Arie Levant. Principles of 2-sliding mode design. *Automatica*, 43(4), 2007.

[15] Kristian Løkken. Adaptive backstepping with application with electro-pneumatic clutch actuators. Master's thesis, Norwegian University of Science and Technology, 2006.

[16] Jean-Jacques E. Slotine and Weiping Li. *Applied Nonlinear Control.* Prentice Hall Inc., 1991.

[17] K. David Young, Vadim I. Utkin, and Ümit Özgüner. A control engineer's guide to sliding mode control. *IEEE Transactions on Control Systems Technology*, 7(3), 1999.

[18] Gjert Ørbeck Vallevik. Adaptive nonlinear observer for electropneumatic clutch actuation. Master's thesis, Norwegian University of Science and Technology, 2006.

Appendix A

Simulation model parameters

Table A.1: Simulation model parameters.

Constant name	Value	Description
T_0	293 K	Initial/environmental temperature
T_{inA}	T_0 K	Temperature of inlet air to chamber A
T_{inB}	T_0 K	Temperature of inlet air to chamber B
T_{A0}	T_0 K	Initial temperature chamber A
T_{B0}	T_0 K	Initial temperature chamber B
P_0	10^5 Pa	Environmental pressure
P_E	P_0 Pa	Exhaust pressure
P_S	$9 \cdot 10^5$ Pa	Supply pressure
R	287.05 J/kgK	Dry air gas constant
ρ_0	1.185 kg/m^3	Air density
r_{act}	0.125/2 m	Actuator piston radius
A_A	$\pi \cdot \mathrm{r}_{\mathrm{act}}^2$ m^2	Actuator piston area, side A
A_B	0.0122 m^2	Actuator piston area, side B
A_0	$1.1310 \cdot 10^{-4}$ m^2	Area of the moving part of the actuator exposed to environmental pressure
M	10 kg	Equivalent mass actuator
y_0	0 m	Initial clutch actuator position
v_0	0 m/s	Initial clutch actuator speed
V_A0	$1.48 \cdot 10^{-4}$ m^3	Initial volume chamber A
V_{B0}	$0.57 \cdot 10^{-3}$ m^3	Initial volume chamber B
B_0	0.528	Critical pressure ratio
C_r	$2.1173 \cdot 10^{-8}$ m^3/Pas	Flow conductance of the exhaust restriction
B_r	-0.7596	Parameter in the flow rate model of chamber B

Table A.2: Simulation model parameters.

Constant name	Value	Description
C_{vs}	$21.7 \cdot -9$ m^3/Pas	Supply valve flow conductance
C_{ve}	$30 \cdot 10^{-9}$ m^3/Pas	Exhaust valve flow conductance
T_{pwm}	0.01 s	Pulse period Pulse-width modulation
L_w	$2 \cdot \pi \cdot \mathrm{r_{act}}$ m	Actuator piston perimeter
κ	1.4	Ratio of specific heats
A_{wA0}	0.078 m^2	Effective area of heat transfer at $y = 0$
A_{wB0}	$10^{-}4$ m^2	Effective area of heat transfer at $y = 0$
H_w	10.16 W/m^{2}K	Empirical convective heat coefficient
T_w	$\mathrm{T_0}$ K	Cylinder wall temperature
D_v	5000 Ns/m	Viscous damping coefficient
K_z	$1 \cdot 10^6$ N/m	Deflection stiffness
$D_{\dot{z}}$	5000 Ns/m	Deflection damping coefficient
F_C	200 N	Coulomb friction level
z_0	0 m	Initial pre-sliding displacement

Appendix B

Mathematical results

B.1 Realization of the low pass filter differentiator

In this section the realization of the linear filter and differentiator in Section 3.1 is performed. The derivation of the realization of the PD controller in Section 4.6 and this filter is analogous, therefore only the filter realization is covered in detail. The algorithm is given in [2]. The filter equation is given by

$$h_f(s) = \frac{s}{1+Ts} \tag{B.1}$$

The transfer function is going to be separated in a constant $h_f(\infty)$, and a strictly proper term $h_{f,sp}(s)$

$$h_f(s) = h_f(\infty) + h_{f,sp}(s) \tag{B.2}$$

$$\begin{aligned} h_f(\infty) &= \lim_{s\to\infty} h_f(s) \\ &= \lim_{s\to\infty} \frac{1}{\frac{1}{s}+T} \\ &= \frac{1}{T} \end{aligned} \tag{B.3}$$

The strictly proper part is given by

$$\begin{aligned} h_{f,sp} &= h(s) - h(\infty) \\ &= \frac{s}{1+Ts} - \frac{1}{T} \\ &= \frac{-\frac{1}{T^2}}{\frac{1}{T}+s} \end{aligned} \tag{B.4}$$

where the denominator is written in monic form. The terms for the realization can now be identificated and inserted, yielding

$$\dot{x} = -\frac{1}{T}x + u \tag{B.5}$$

$$y = -\frac{1}{T^2}x + \frac{1}{T}u \tag{B.6}$$

where y is the filtered derivative of the filter input u.

B.2 Normal form for sliding mode control

Evaluation of the elements in (4.39)

$$h(\boldsymbol{x}) = y \tag{B.7}$$

$$\begin{aligned} L_f h(\boldsymbol{x}) &= \frac{\partial h(\boldsymbol{x})}{\partial \boldsymbol{x}} f(\boldsymbol{x}) \\ &= \begin{bmatrix} 1 & 0 & 0 \end{bmatrix} \begin{bmatrix} v \\ \cdot \\ \cdot \end{bmatrix} \\ &= v \end{aligned} \tag{B.8}$$

$$\begin{aligned} L_f^2 h(\boldsymbol{x}) &= \frac{\partial L_f h(\boldsymbol{x})}{\partial \boldsymbol{x}} f(\boldsymbol{x}) \\ &= \begin{bmatrix} 0 & 1 & 0 \end{bmatrix} \begin{bmatrix} \cdot \\ \frac{1}{M}(Ap - Ap_0 - f_l(y) - D_v v) \\ \cdot \end{bmatrix} \\ &= \frac{1}{M}(Ap - Ap_0 - f_l(y) - D_v v) \end{aligned} \tag{B.9}$$

yields the expression of a diffeomorphism for this system

$$\boldsymbol{\xi} = T(\boldsymbol{x}) = \begin{bmatrix} y \\ v \\ \frac{1}{M}(Ap - Ap_0 - f_l(y) - D_v v) \end{bmatrix} \tag{B.10}$$

and these are the new system variables.

The nonlinear system equations, $\gamma(\boldsymbol{x})$ and $\alpha(\boldsymbol{x})$, are given by

$$\begin{aligned} \gamma(\boldsymbol{x}) &= L_g L_f^2 h(\boldsymbol{x}) \\ &= \frac{\partial}{\partial \boldsymbol{x}} \left(L_f^2 h(\boldsymbol{x}) \right) g(\boldsymbol{x}) \\ &= \frac{\partial}{\partial \boldsymbol{x}} \left(\frac{1}{M} \left(Ap - Ap_0 - f_l(y) - D_v v \right) \right) \frac{RT_0}{V(y)} \\ &= \frac{1}{M} \begin{bmatrix} -\frac{\partial f_l(y)}{\partial y} & -D_v & A \end{bmatrix} \begin{bmatrix} 0 \\ 0 \\ \frac{RT_0}{V(y)} \end{bmatrix} \\ &= \frac{ART_0}{MV(y)} \end{aligned} \tag{B.11}$$

$$\begin{aligned}
\alpha(\boldsymbol{x}) &= -\frac{L_f^3 h(\boldsymbol{x})}{L_g L_f^3 h(\boldsymbol{x})} \\
&= -\frac{\frac{\partial L_f^2 h(\boldsymbol{x})}{\partial \boldsymbol{x}} f(\boldsymbol{x})}{\gamma(\boldsymbol{x})} \\
&= -\frac{1}{M\gamma(\boldsymbol{x})} \begin{bmatrix} -\frac{\partial f_l(y)}{\partial y} & -D_v & A \end{bmatrix} \begin{bmatrix} v \\ \frac{1}{M}(Ap - Ap_0 - f_l(y) - D_v v) \\ -\frac{A}{V(y)} vp \end{bmatrix} \\
&= -\frac{1}{M\gamma(\boldsymbol{x})} \left(-\frac{\partial f_l(y)}{\partial y} v - \frac{D_v}{M} \left(Ap - Ap_0 - f_l(y) - D_v v\right) - \frac{A^2}{V(y)} vp \right)
\end{aligned} \tag{B.12}$$

The clutch load force $f_l(y)$ is given in Section 2.1.3, equations (2.12) - (2.14). The derivative is straightforward to calculate because it is given by polynomials.

$$f_l(y) = \boldsymbol{\theta}_l^T \boldsymbol{\phi}_l(y) \tag{B.13}$$

$$\frac{\partial f_l(y)}{\partial y} = \boldsymbol{\theta}_l^T \frac{\partial \boldsymbol{\phi}_l}{\partial y} \tag{B.14}$$

$$\frac{\partial \phi_{l1}}{\partial y} = \begin{cases} 0, & y < t_1 \\ 1, & t_1 \leq y < t_2 \\ -153.85y + 1.3077, & t_2 \leq y < t_3 \\ 0, & y > t_3 \end{cases} \tag{B.15}$$

$$\frac{\partial \phi_{l2}}{\partial y} = \begin{cases} 0, & y < t_2 \\ 0.1538y - 3.0769 \cdot 10^{-4}, & t_2 \leq y < t_3 \\ 1, & y > t_3 \end{cases} \tag{B.16}$$

$$\frac{\partial \phi_{l3}}{\partial y} = \begin{cases} 0, & y < t_2 \\ -6998.1y^2 + 94.47y - 0.1610, & t_2 \leq y < t_4 \\ 6998.1y^2 - 227.43y + 1.6900, & t_4 \leq y < t_5 \\ 0, & y \geq t_5 \end{cases} \tag{B.17}$$

The clutch load function, its derivative and basis functions are shown in Figure 2.2.

By combining (4.36) and (4.38), it is seen that

$$\begin{aligned}
\dot{\boldsymbol{\xi}}_3 &= f(\boldsymbol{\xi}) + g(\boldsymbol{\xi})u \\
&= \gamma(\boldsymbol{x})[u - \alpha(\boldsymbol{x})] \\
&= -\gamma(\boldsymbol{x})\alpha(\boldsymbol{x}) + \gamma(\boldsymbol{x})u
\end{aligned} \tag{B.18}$$

and inserting (B.11) and (B.12) yield

$$\begin{aligned}\dot{\boldsymbol{\xi}}_3 &= \frac{1}{M}\left(-\frac{\partial f_l(y)}{\partial y}v - \frac{D_v}{M}\left(Ap - Ap_0 - f_l(y) - D_v v\right) - \frac{A^2}{V(y)}vp\right) \\ &\quad + \frac{ART_0}{MV(y)}u \\ &= \frac{1}{M}\left(-\frac{\partial f_l(\xi_1)}{\partial \xi_1}\xi_2 - \frac{D_v}{M}\xi_3 - \frac{A}{V(\xi_1)}\xi_2(M\xi_3 + Ap_0 + f_l(\xi_1) + D_v\xi_2)\right) \\ &\quad + \frac{ART_0}{MV(\xi_1)}u\end{aligned} \tag{B.19}$$

where the last equality is obtained by isolating and inserting p from (4.2).

Appendix C

Additional plots

C.1 Filter plots

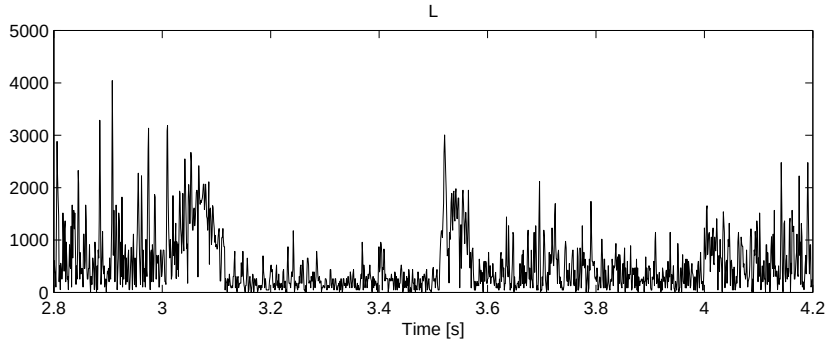

Figure C.1: Lipschitz constant estimate, $L(t) = 4\sqrt{y^2 + \dot{y}^2 + \ddot{y}^2 + 10}$ applied to position measurement. ODE1, step size 0.001 s.

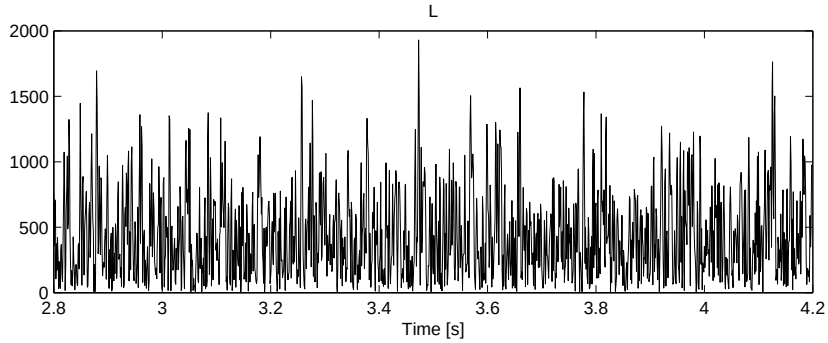

Figure C.2: Lipschitz constant estimate, $L(t) = 4\sqrt{y^2 + \dot{y}^2 + \ddot{y}^2 + 10}$, applied to simulation results. ODE1, step size 0.001 s.

C.2 Slow fall-off filter test

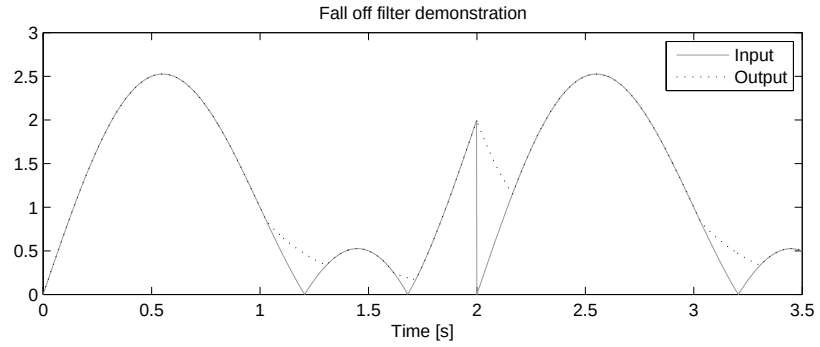

Figure C.3: Slow fall-off filter demonstration. $T_{falloff} = 0.3$ s.

C.3 Controller testing

C.3.1 Ideal sliding mode controller

Figure C.4 - C.7 show simulation results of time segment, when the ideal sliding mode controller from Section 4.7.2 is applied.

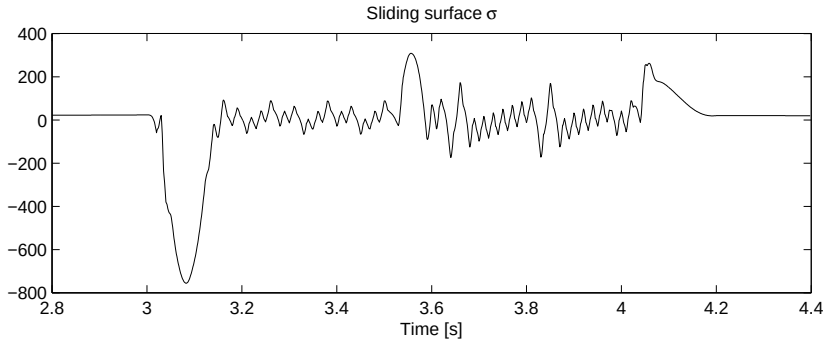

Figure C.4: Sliding surface. ODE1, step size 0.001 s.

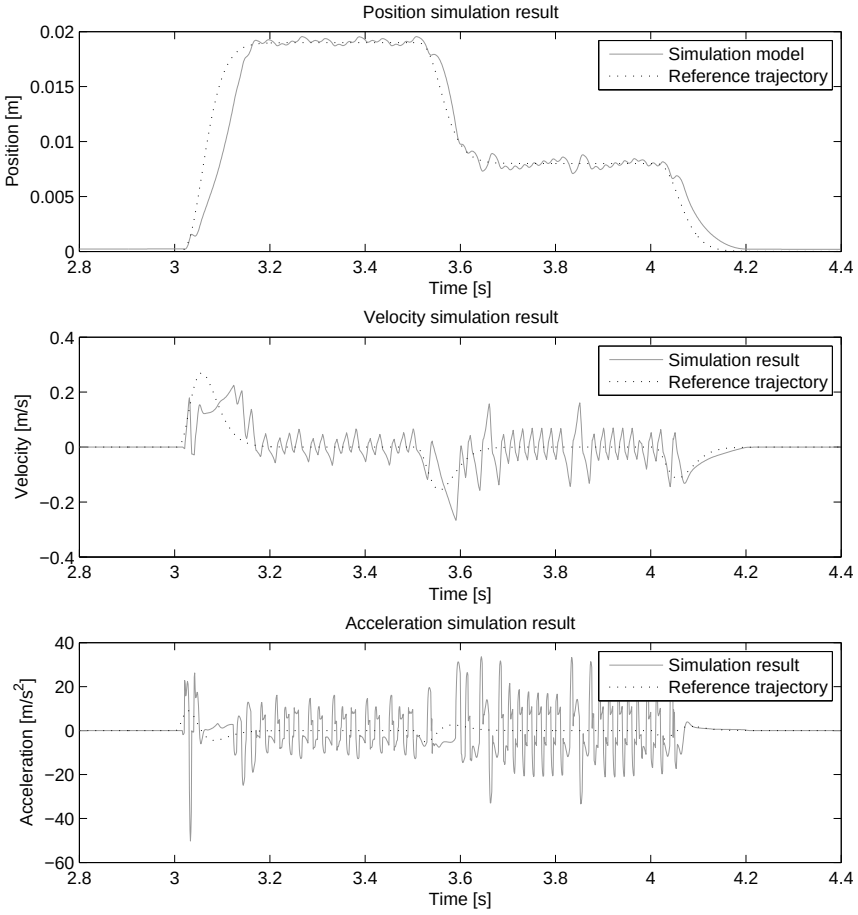

Figure C.5: Simulation results and reference trajectories for position, velocity and acceleration. ODE1, step size 0.001 s.

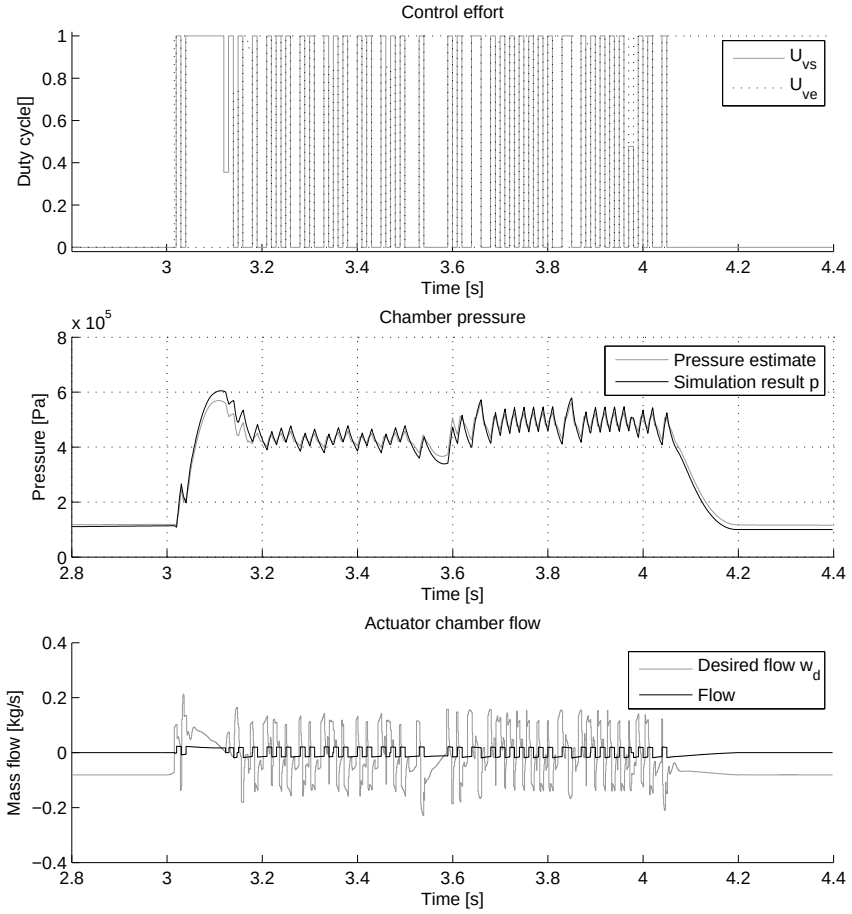

Figure C.6: Control input, chamber pressure and mass flow. ODE1, step size 0.001 s.

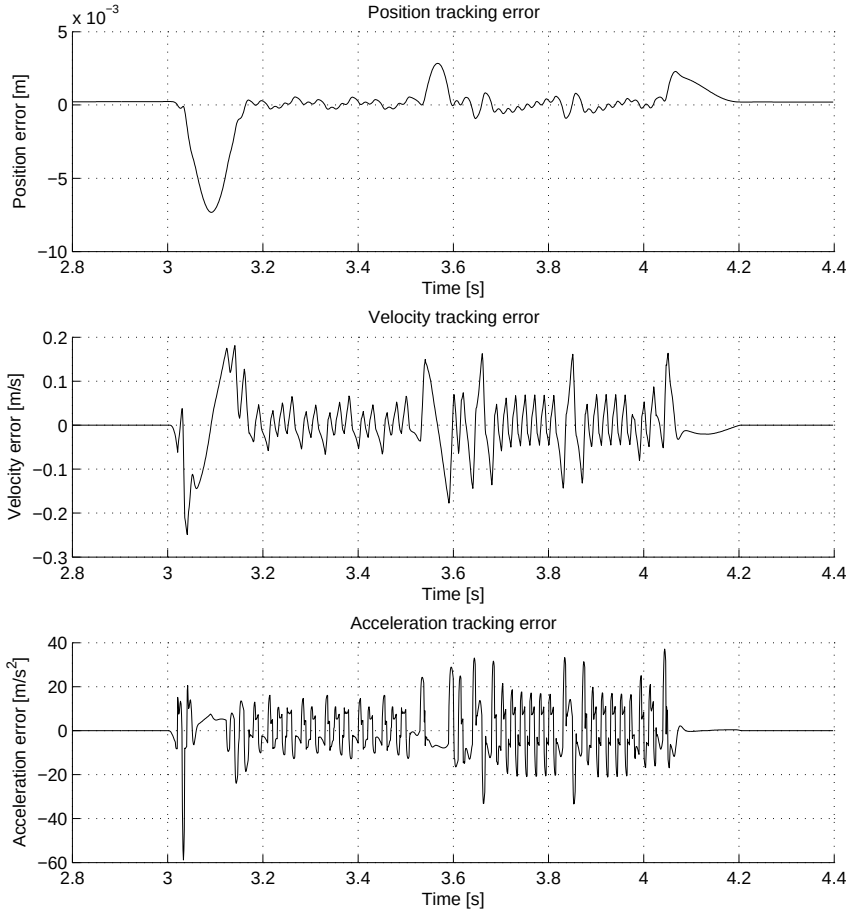

Figure C.7: Tracking error in position, velocity and acceleration. ODE1, step size 0.001 s.

C.3.2 Variable boundary layer controller testing with slower reference filter

Figure C.8 shows tracking position, velocity and acceleration for the VBLSM controller with reference trajectory filter time constant 0.1 s. Measurement noise is enabled.

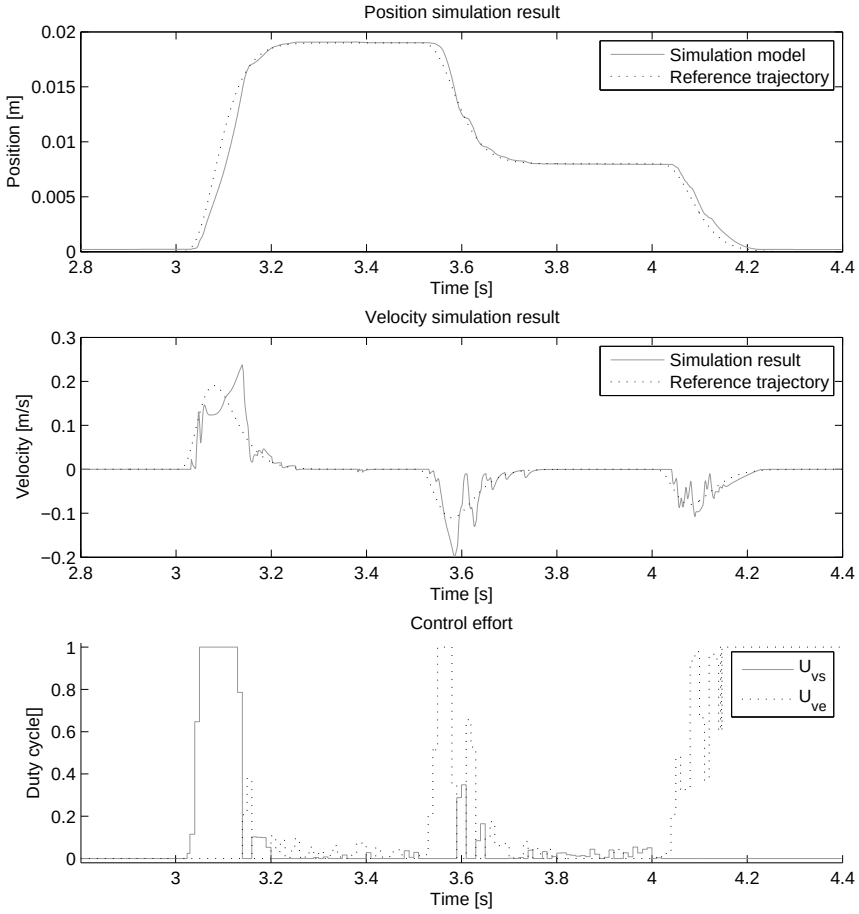

Figure C.8: Tracking error in position, velocity and acceleration. ODE1, step size 0.001 s. VBLSM controller, time constant 0.1 s in reference trajectory filter.

Appendix D

Simulink diagrams

This chapter contains diagrams of the implementation of the system in Matlab Simulink.

D.1 Controller disengage block

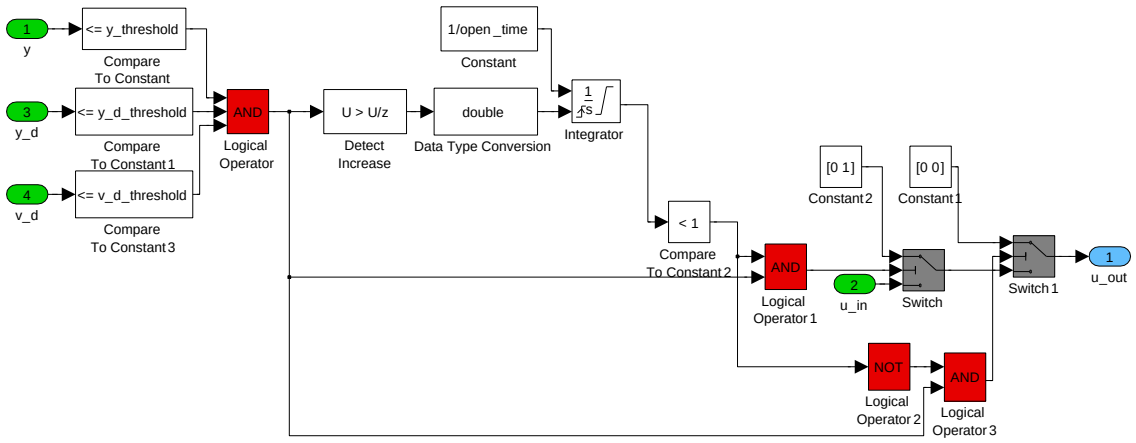

Figure D.1: Controller disengage block implemented in Matlab Simulink.

D.2 Measurement filter implementation

D.2.1 Levant differentiator

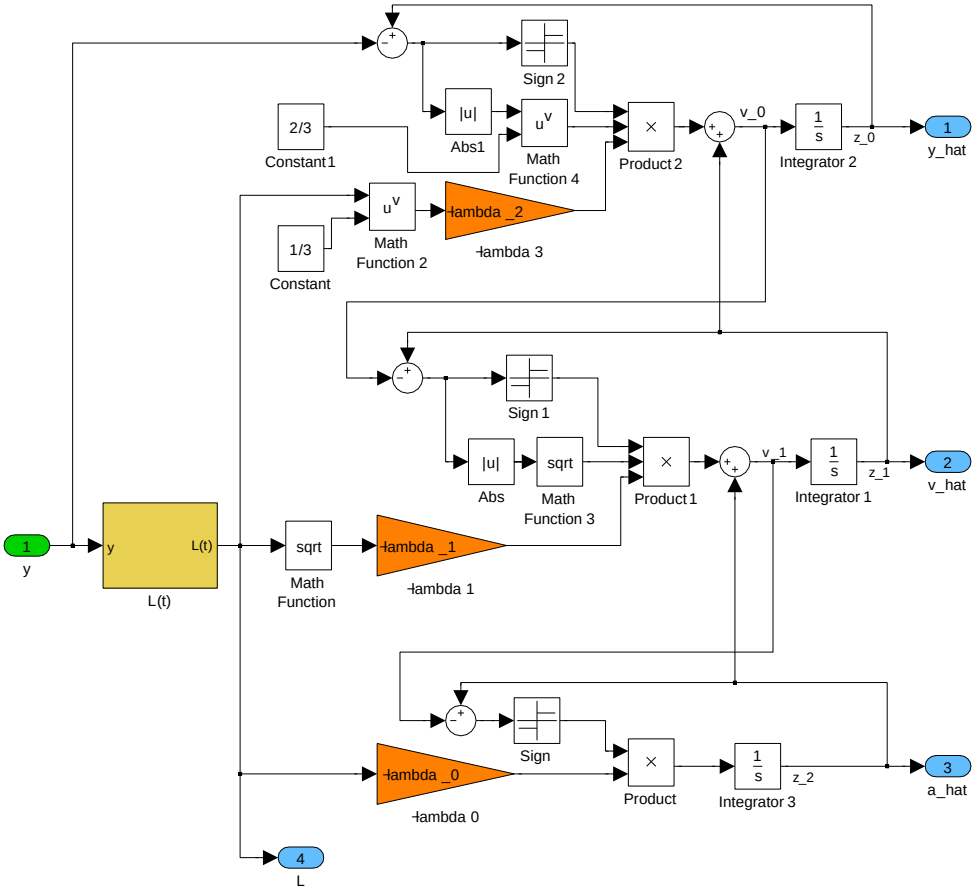

Figure D.2: Levant differentiator implemented in Matlab Simulink.

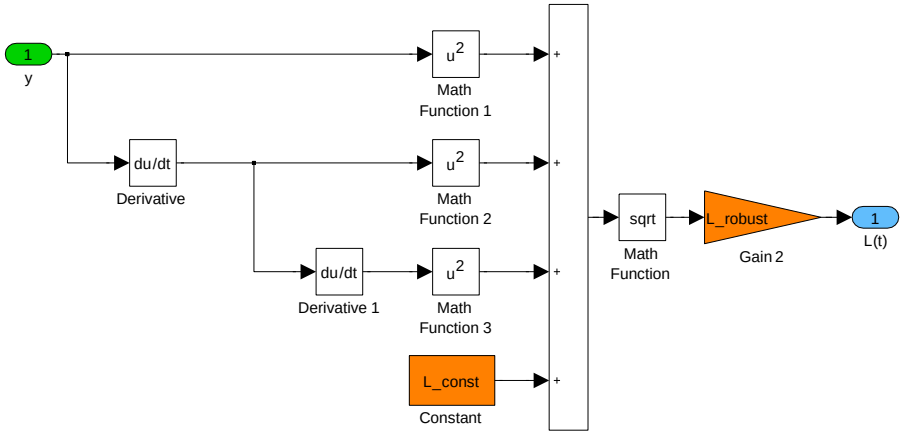

Figure D.3: $L(t)$ for the Levant differentiator, implemented in Matlab Simulink.

D.2.2 Low pass filter differentiator

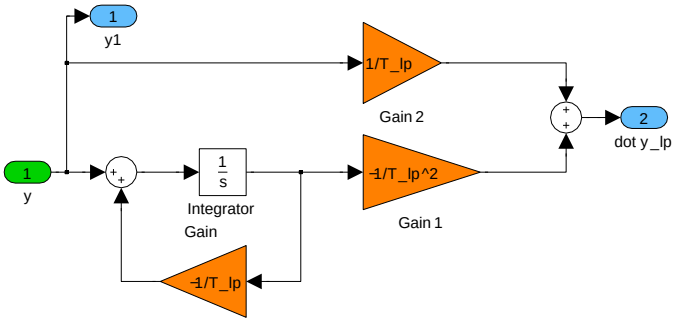

Figure D.4: Low pass filter-differentiator implemented in Matlab Simulink.

D.3 Controller implementation for field test

The block called `MABX: 1713-RTtruck` contains the connections to the clutch actuator system onboard the test truck. The `ValveUsageReduser` blocks ensures that the valves are sufficiently held at rest after a certain usage to avoid overheating.

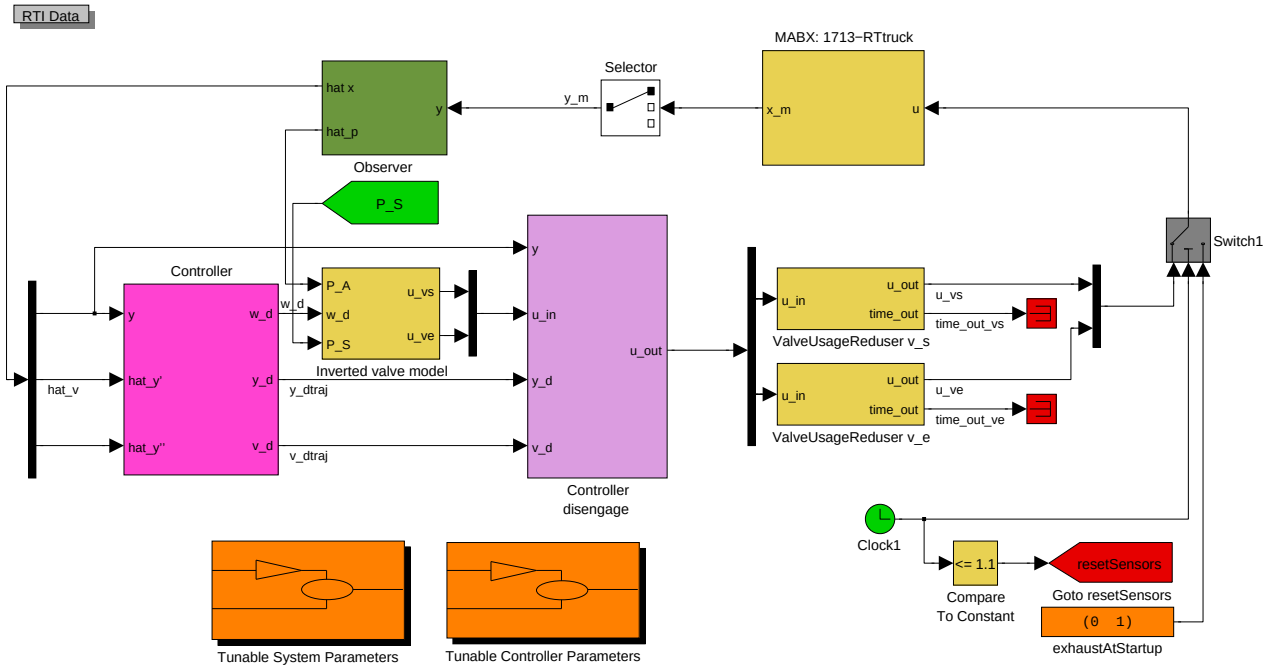

Figure D.5: Controller implemented in Simulink for cross-compilation and application on the dSpace control unit.